

QuickPol: Fast calculation of effective beam matrices for CMB polarization

Eric Hivon¹, Sylvain Mottet¹ & Nicolas Ponthieu^{2,3}

¹ Sorbonne Universités, UPMC Univ. Paris 6 & CNRS (UMR7095): Institut d’Astrophysique de Paris, 98 bis Boulevard Arago, F-75014, Paris, France

² Institut de Planétologie et d’Astrophysique de Grenoble, Université Grenoble Alpes, CNRS (UMR5274), F-38000, Grenoble, France

³ Institut d’Astrophysique Spatiale, CNRS (UMR8617) Université Paris-Sud 11, Bâtiment 121, F-91405, Orsay, France

Received Aug 31, 2016 / Accepted Oct 03, 2016

ABSTRACT

Current and planned observations of the cosmic microwave background (CMB) polarization anisotropies, with their ever increasing number of detectors, have reached a potential accuracy that requires a very demanding control of systematic effects. While some of these systematics can be reduced in the design of the instruments, others will have to be modeled and hopefully accounted for or corrected *a posteriori*. We propose QuickPol, a quick and accurate calculation of the full effective beam transfer function and of temperature to polarization leakage at the power spectra level, as induced by beam imperfections and mismatches between detector optical and electronic responses. All the observation details such as exact scanning strategy, imperfect polarization measurements, and flagged samples are accounted for. Our results are validated on *Planck* high frequency instrument (HFI) simulations. We show how the pipeline can be used to propagate instrumental uncertainties up to the final science products, and could be applied to experiments with rotating half-wave plates.

Key words. Cosmology, polarization, systematic effects

1. Introduction

We are now entering an era of precise measurements of the cosmic microwave background (CMB) polarization, with potentially enough sensitivity to detect or even characterize the primordial tensorial B modes, the smoking gun of inflation (e.g., Zaldarriaga & Seljak (1997) and references therein). This raises expectations about the control and the correction of contaminations by astrophysical foregrounds, observational features, and instrumental imperfections. As it has in the past, progress will come from the synergy between instrumentation and data analysis. Improvements in instrumentation call for improved precision in final results, which are made possible by improved algorithms and the ability to deal with more and more massive data sets. In turn, expertise gained in data processing allows for better simulations that lead to new instrument designs and better suited observations. An example of such joint developments is the study of the impact of optics- and electronics-related imperfections on the measured CMB temperature and polarization angular power spectra and their statistical isotropy. Systematic effects such as beam non-circularity, response mismatch in dual polarization measurements and scanning strategy imperfections, as well as how they can be mitigated, have been extensively studied in the preparation of forthcoming instruments (including, but not limited to Souradeep & Ratra 2001; Fosalba et al. 2002; Hu et al. 2003; Mitra et al. 2004, 2009; O’Dea et al. 2007; Rosset et al. 2007; Shimon et al. 2008; Miller et al. 2009a,b; Hanson et al. 2010; Leahy et al. 2010; Rosset et al. 2010; Ramamonjisoa et al. 2013; Rathaus & Kovetz 2014; Wallis et al. 2014; Pant et al. 2016), and during the analysis of data collected by WMAP¹ (Smith et al. 2007; Hinshaw et al. 2007; Page et al. 2007) or *Planck*² (Planck 2013-VII 2014; Planck 2013-XVII 2014; Planck 2015-XI 2016) satellite missions.

At the same time, several deconvolution algorithms and codes have been proposed to clean up the CMB maps from such beam-related effects prior to the computation of the power spectra, like PreBeam (Armitage-Caplan & Wandelt 2009), ArtDeco (Keihänen & Reinecke 2012), and in Bennett et al. (2013) and Wallis et al. (2015).

Finally, in a related effort, the FEBeCoP pipeline, described in Mitra et al. (2011) and used in *Planck* data analysis (Planck 2013-IV 2014; Planck 2013-VII 2014), can be seen as a convolution facility, by providing, at arbitrary locations on the sky, the effective beam maps and point spread functions of a detector set, which, in turn, can be used for a Monte-Carlo based description of the effective beam window functions for a given sky model.

In this paper, we introduce the QuickPol pipeline, an extension to polarization of the Quickbeam algorithm used in Planck 2013-VII (2014). It allows a quick and accurate computation of the leakage and cross-talk between the various temperature and polarization power spectra (TT , EE , BB , TE , etc.) taking into account the exact scanning, sample flags, relative weights,

Send offprint requests to: hivon@iap.fr

¹ Wilkinson microwave anisotropy probe: <http://map.gfsc.nasa.gov>.

² <http://www.esa.int/Planck>.

and scanning beams of the considered set(s) of detectors. The end results are effective beam matrices describing, for each multipole ℓ , the mixing of the various spectra, independently of the actual value of the spectra. As we shall see, the impact of changing any time-independent feature of the instrument, such as its beam maps, relative gain calibrations, detector orientations, and polarization efficiencies can be propagated within seconds to the final beam matrices products, allowing extremely fast Monte-Carlo exploration of the experimental features. QuickPol is thus a powerful tool for both real data analysis and forthcoming experiments, simulations and design.

The paper is organized as follows. The mathematical formalism is exposed in Section 2 and analytical results are given in Section 3. The numerical implementation is detailed in Section 4 and compared to the results of *Planck* simulations in Section 5. Section 6 shows the propagation of instrumental uncertainties. We discuss briefly the case of rotating half-wave plates in Section 7 and conclude in Section 8.

2. Formalism

2.1. Data stream of a polarized detector

As usual in the study of polarization measurement, we will use Jones' formalism to study the evolution of the electric component of an electro-magnetic radiation in the optical system. Let us consider a quasi monochromatic³ radiation propagating along the z axis, and hitting the optical system at a position $\mathbf{r} = \begin{pmatrix} x \\ y \end{pmatrix}$. The incoming electric field $\mathbf{e}(\mathbf{r}) = \begin{pmatrix} e_x \\ e_y \end{pmatrix} e^{ik(z-ct)}$ will be turned into $\mathbf{e}'(\mathbf{r}) = \mathbf{J}(\mathbf{r}) \cdot \mathbf{e}(\mathbf{r})$, where $\mathbf{J}(\mathbf{r})$ is the 2x2 complex Jones matrix of the system.

A rotation of the optical system by α around the z axis can be seen as a rotation of both the orientation and location of the incoming radiation by $-\alpha$ in the detector reference frame, and the same input radiation is now received as

$$\mathbf{e}'(\alpha, \mathbf{r}) = \mathbf{J}(\mathbf{r}_\alpha) \cdot \mathbf{R}_\alpha^\dagger \cdot \mathbf{e}(\mathbf{r}), \quad (1)$$

with

$$\mathbf{r}_\alpha = \mathbf{R}_\alpha^\dagger \cdot \mathbf{r}, \quad (2)$$

$$\mathbf{R}_\alpha = \begin{pmatrix} \cos \alpha & -\sin \alpha \\ \sin \alpha & \cos \alpha \end{pmatrix}, \quad (3)$$

and the \dagger sign representing the adjoint operation, which for a real rotation matrix, simply amounts to the matrix transpose. The measured signal is

$$d(\alpha) = \int d\mathbf{r} d(\alpha, \mathbf{r}) \quad (4)$$

with

$$\begin{aligned} d(\alpha, \mathbf{r}) &= \langle \mathbf{e}'^\dagger \cdot \mathbf{e}' \rangle = \langle \text{Tr}(\mathbf{e}' \cdot \mathbf{e}'^\dagger) \rangle \\ &= \text{Tr}(\mathbf{J}(\mathbf{r}_\alpha) \cdot \mathbf{R}_\alpha^\dagger \cdot \langle \mathbf{e} \cdot \mathbf{e}^\dagger \rangle \cdot \mathbf{R}_\alpha \cdot \mathbf{J}^\dagger(\mathbf{r}_\alpha)). \end{aligned} \quad (5)$$

We now introduce the Stokes parameters of the input signal (dropping the dependence on \mathbf{r})

$$\langle \mathbf{e} \cdot \mathbf{e}^\dagger \rangle = \frac{1}{2} \begin{pmatrix} T + Q & U + iV \\ U - iV & T - Q \end{pmatrix} \quad (6)$$

and of the (un-rotated) instrument response

$$\mathbf{J}^\dagger \cdot \mathbf{J} = \frac{1}{2} \begin{pmatrix} \tilde{T} + \tilde{Q} & \tilde{U} - i\tilde{V} \\ \tilde{U} + i\tilde{V} & \tilde{T} - \tilde{Q} \end{pmatrix}, \quad (7)$$

to obtain

$$d(\alpha) = \frac{1}{2} \int d\mathbf{r} [\tilde{T}(\alpha, \mathbf{r})T(\mathbf{r}) + \tilde{Q}(\alpha, \mathbf{r})Q(\mathbf{r}) + \tilde{U}(\alpha, \mathbf{r})U(\mathbf{r}) - \tilde{V}(\alpha, \mathbf{r})V(\mathbf{r})]. \quad (8)$$

With the rotated instrument response:

$$\tilde{T}(\alpha, \mathbf{r}) = \tilde{T}(\mathbf{r}_\alpha), \quad (9a)$$

$$\tilde{Q}(\alpha, \mathbf{r}) = \tilde{Q}(\mathbf{r}_\alpha) \cos 2\alpha - \tilde{U}(\mathbf{r}_\alpha) \sin 2\alpha, \quad (9b)$$

$$\tilde{U}(\alpha, \mathbf{r}) = \tilde{Q}(\mathbf{r}_\alpha) \sin 2\alpha + \tilde{U}(\mathbf{r}_\alpha) \cos 2\alpha, \quad (9c)$$

$$\tilde{V}(\alpha, \mathbf{r}) = \tilde{V}(\mathbf{r}_\alpha). \quad (9d)$$

³ Although it is important when trying to disentangle sky signals with different electromagnetic spectra (Planck 2013-VI 2014), the finite bandwidth of the actual detectors only plays a minor role in the problem considered here, and will be ignored in this paper.

Following Rosset et al. (2010), we can specify the instrument as being a beam forming optics, followed by an imperfect polarimeter in the direction x , with $0 \leq \eta \leq 1$, and having an overall optical efficiency $0 \leq \tau \leq 1$:

$$\mathbf{J}(\mathbf{r}) = \sqrt{\tau} \begin{pmatrix} 1 & 0 \\ 0 & \sqrt{\eta} \end{pmatrix} \begin{pmatrix} b_{xx}(\mathbf{r}) & b_{xy}(\mathbf{r}) \\ b_{yx}(\mathbf{r}) & b_{yy}(\mathbf{r}) \end{pmatrix}, \quad (10)$$

with

$$\begin{pmatrix} b_{ax}^* \\ b_{ay}^* \end{pmatrix} \cdot (b_{ax} \ b_{ay}) = \frac{1}{2} \begin{pmatrix} \tilde{I}_a + \tilde{Q}_a & \tilde{U}_a - i\tilde{V}_a \\ \tilde{U}_a + i\tilde{V}_a & \tilde{I}_a - \tilde{Q}_a \end{pmatrix} \quad (11)$$

for $a = x, y$. The Stokes parameters of the instrument are then $\tilde{\mathbf{S}} = \tau(\tilde{\mathbf{S}}_x + \eta\tilde{\mathbf{S}}_y)$ for $\tilde{\mathbf{S}} = \tilde{I}, \tilde{Q}, \tilde{U}, \tilde{V}$.

If the beam is assumed to be perfectly co-polarized, that is, it does not alter at all the polarization of the incoming radiation, with $b_{xy} = b_{yx} = 0$ and $b_{xx} = b_{yy}$, then $\tilde{U}_x = \tilde{U}_y = \tilde{V}_x = \tilde{V}_y = 0$, $\tilde{I}_x = \tilde{I}_y = \tilde{Q}_x = -\tilde{Q}_y$, and $\tilde{I} = (1 + \eta)\tilde{I}_x$, $\tilde{Q} = (1 - \eta)\tilde{Q}_x$, $\tilde{U} = \tilde{V} = 0$, Eqs. (8, 9) become

$$d(\alpha) = \frac{1 + \eta}{2} \tau \int d\mathbf{r} \tilde{I}_x(\mathbf{r}_\alpha) [T(\mathbf{r}) + \rho(Q(\mathbf{r}) \cos 2\alpha + U(\mathbf{r}) \sin 2\alpha)], \quad (12)$$

where

$$\rho = \frac{1 - \eta}{1 + \eta} \quad (13)$$

is the polar efficiency, such that $0 \leq \rho \leq 1$ with $\rho = 1$ for a perfect polarimeter and $\rho = 0$ for a detector only sensitive to intensity. In the case of *Planck* high frequency instrument (HFI), Rosset et al. (2010) showed the measured polarization efficiencies to differ by $\Delta\rho' = 1\%$ to 16% from their ideal values, with an absolute statistical uncertainty generally below 1%. The particular case of co-polarized beams is important because in most experimental setups, such as *Planck*, the beam response calibration is done on astronomical or artificial far field sources. Well known, compact, and polarized sources are generally not available to measure \tilde{Q} and \tilde{U} and only the intensity beam response \tilde{I} is measured. In the absence of reliable physical optics modeling of the beam response, one therefore has to assume \tilde{Q} and \tilde{U} to be perfectly co-polarized.

So far, we have only considered the optical beam response. We should also take into account the scanning beam, which is the convolution of the optical beam with the finite time response of the instrument (or its imperfect correction) as it moves around the sky, as described in Planck 2013-VII (2014) and Planck 2015-VII (2016). These time related effects can be a major source of elongation of the scanning beams, and can increase the beam mismatch among sibling detectors. If one assumes the motion of the detectors on the sky to be nearly uniform, as was the case for *Planck*, then optical beams can readily be replaced by scanning beams in the QuickPol formalism.

2.2. Spherical harmonics analysis

We now define the tools that are required to extend the above results to the full celestial sphere. The temperature T is a scalar quantity, while the linear polarization $Q \pm iU$ is of spin ± 2 , and the circular polarization V is generally assumed to vanish. They can be written as linear combinations of spherical harmonics (SH):

$$T(\mathbf{r}) = \sum_{\ell m} a_{\ell m}^T Y_{\ell m}(\mathbf{r}), \quad (14)$$

$$Q(\mathbf{r}) \pm iU(\mathbf{r}) = \sum_{\ell m} {}_{\pm 2}a_{\ell m} {}_{\pm 2}Y_{\ell m}(\mathbf{r}), \quad (15)$$

although one usually prefers the scalar and fixed parity E and B components

$$a_{\ell m}^E \pm ia_{\ell m}^B = -{}_{\pm 2}a_{\ell m} \quad (16)$$

such that $a_{\ell m}^{X*} = (-1)^m a_{\ell -m}^X$ for $X = T, E, B$. In other terms

$$\begin{pmatrix} 0a_{\ell m} \\ 2a_{\ell m} \\ -2a_{\ell m} \end{pmatrix} = \mathbf{R}_2 \cdot \begin{pmatrix} a_{\ell m}^T \\ a_{\ell m}^E \\ a_{\ell m}^B \end{pmatrix} \quad (17)$$

with

$$\mathbf{R}_2 = \begin{pmatrix} 1 & 0 & 0 \\ 0 & -1 & -i \\ 0 & -1 & i \end{pmatrix}. \quad (18)$$

The sign convention used in Eq. (16) is consistent with Zaldarriaga & Seljak (1997) and the HEALPix⁴ library (Górski et al. 2005).

⁴ <http://healpix.sourceforge.net>.

The response of a beam centered on the North pole can also be decomposed in SH coefficients

$$b_{\ell m} = \int d\mathbf{r} \tilde{I}(\mathbf{r}) Y_{\ell m}^*(\mathbf{r}), \quad (19)$$

$$\pm_2 b_{\ell m} = \int d\mathbf{r} (\tilde{Q}(\mathbf{r}) \pm i\tilde{U}(\mathbf{r})) \pm_2 Y_{\ell m}^*(\mathbf{r}), \quad (20)$$

while the coefficients of a rotated beam can be computed by noting that under a rotation of angle α around the direction \mathbf{r} , the SH of spin s transform as

$${}_s Y_{\ell m}(\mathbf{r}') \longrightarrow \sum_{m'} {}_s Y_{\ell m'}(\mathbf{r}') D_{m'm}^\ell(\mathbf{r}, \alpha). \quad (21)$$

The elements of Wigner rotation matrices D are related to the SH via (Challinor et al. 2000)

$$D_{m'm}^\ell(\mathbf{r}, \alpha) = (-1)^m q_\ell {}_{-m} Y_{\ell m'}^*(\mathbf{r}) e^{-im\alpha}, \quad (22)$$

with $q_\ell = \sqrt{\frac{4\pi}{2\ell+1}}$.

If the beam is assumed to be co-polarized and coupled with a perfect polarimeter rotated by an angle γ , such that $\tilde{Q} + i\tilde{U} = \tilde{I} e^{2i\gamma}$ in cartesian coordinates (or $\tilde{Q} + i\tilde{U} = \tilde{I} e^{2i(\gamma-\phi)}$ in (θ, ϕ) polar coordinates), simple relations between $b_{\ell m}$ and $\pm_2 b_{\ell, m}$ can be established. For a Gaussian circular beam of full width half maximum (FWHM) $\theta_{\text{FWHM}} = \sigma \sqrt{8 \ln 2} \approx 2.355\sigma$ and of throughput $\int d\mathbf{r} \tilde{I}(\mathbf{r}) = \sqrt{4\pi} b_{00} = 1$, Challinor et al. (2000) found

$$b_{\ell m} = \sqrt{\frac{2\ell+1}{4\pi}} e^{-\frac{1}{2}\ell(\ell+1)\sigma^2} \delta_{m,0}, \quad (23a)$$

$$\pm_2 b_{\ell, m} = b_{\ell, m \pm 2} e^{2\sigma^2} e^{\pm 2i\gamma}. \quad (23b)$$

The factor $c_2 = e^{2\sigma^2}$ in Eq. (23b) is such that $c_2 - 1 < 1.1 \cdot 10^{-4}$ for $\theta_{\text{FWHM}} \leq 1^\circ$ and $c_2 - 1 < 3.1 \cdot 10^{-6}$ for $\theta_{\text{FWHM}} \leq 10'$, and will be assumed to be $c_2 = 1$ from now on. For a slightly elliptical Gaussian beam, Fosalba et al. (2002) found

$$\pm_2 b_{\ell, m} = b_{\ell, m \pm 2} e^{\pm 2i\gamma}, \quad (24)$$

while we show in Appendix G that Eq. (24) is true for arbitrarily shaped co-polarized beams. This result can also be obtained by noting that an arbitrary beam is the sum of Gaussian circular beams with different FWHM and center (Tristram et al. 2004), each of them obeying Eq. (23b).

The detector associated to a beam is an imperfect polarimeter with a polarization efficiency ρ' and the overall polarized response of the detector, in a referential *aligned* with its direction of polarization (the so-called Pxx coordinates in *Planck* parlance), reads

$$\tilde{Q} = \rho' \tilde{I}, \quad (25)$$

so that

$$\pm_2 b_{\ell, m} = \rho' b_{\ell, m \pm 2}. \quad (26)$$

We introduced ρ' to distinguish it from the ρ value used in the map-making, as described below.

2.3. Map making equation

A polarized detector pointing, at time t , in the direction \mathbf{r}_t on the sky, and being sensitive to the polarization with angle α_t with respect to the local meridian, measures

$$d(\mathbf{r}_t, \alpha_t) = \int d\mathbf{r}' [\tilde{I}(\mathbf{r}_t, \alpha_t; \mathbf{r}') T(\mathbf{r}') + \tilde{Q}(\mathbf{r}_t, \alpha_t; \mathbf{r}') Q(\mathbf{r}') + \tilde{U}(\mathbf{r}_t, \alpha_t; \mathbf{r}') U(\mathbf{r}')]. \quad (27)$$

The factor $1/2$ present in Eq. (8) is assumed to be absorbed in the gain calibration, performed on large scale temperature fluctuations, such as the CMB solar dipole (Planck 2013-VIII 2014), and we assumed the circular polarization V to vanish. With the definitions introduced in Section 2.2, this becomes

$$d(\mathbf{r}_t, \alpha_t) = \sum_{\ell m s} [{}_0 a_{\ell m} {}_0 b_{\ell s}^* + 1/2 ({}_2 a_{\ell m} {}_2 b_{\ell s}^* + {}_{-2} a_{\ell m} {}_{-2} b_{\ell s}^*)] (-1)^s q_\ell e^{is\alpha_t} {}_{-s} Y_{\ell m}(\mathbf{r}_t). \quad (28)$$

The map-making formalism is set ignoring the beam effects, assuming a perfectly co-polarized detector and an instrumental noise n (Tristram et al. 2011, and references therein), so that, for a detector j , Eq. (12) becomes

$$d_j(t) = T(p) + \rho_j Q(p) \cos 2\alpha_t^{(j)} + \rho_j U(p) \sin 2\alpha_t^{(j)} + n_j(t), \quad (29)$$

where the leading prefactors are here again absorbed in the gain calibration. Let us rewrite it as

$$d_j(t) = A_{t,p}^{(j)} m(p) + n_j(t), \quad (30)$$

with (Shimon et al. 2008)

$$A_{t,p}^{(j)} = \left(1, \rho_j e^{-2i\alpha_t^{(j)}}, \rho_j e^{2i\alpha_t^{(j)}} \right), \quad (31)$$

$$m(p) = (T, P/2, P^*/2)^T, \quad (32)$$

and $P = Q + iU$. Assuming the noise to be uncorrelated between detectors, with covariance matrix $\mathbf{N}_j = \langle \mathbf{n}_j \cdot \mathbf{n}_j^T \rangle$ for detector j , the generalized least square solution of Eq. (29) for a set of detectors is

$$\tilde{\mathbf{m}} = \left(\sum_k \mathbf{A}^{(k)\dagger} \cdot \mathbf{N}_k^{-1} \cdot \mathbf{A}^{(k)} \right)^{-1} \cdot \sum_j \mathbf{A}^{(j)\dagger} \cdot \mathbf{N}_j^{-1} \cdot \mathbf{d}_j. \quad (33)$$

Let us now replace the ideal data stream (Eq. 29) with the one obtained for arbitrary beams (Eq. 27) and further assume that the noise is white and stationary with variance σ_j^2 , so that $\mathbf{N}_j^{-1} = 1/\sigma_j^2 = w_j$. Let us also introduce the binary flag $f_{j,t}$ used to reject individual time samples from the map-making process; Eq. (33) then becomes

$$\tilde{\mathbf{m}}(p) \equiv \begin{pmatrix} \tilde{m}(0; p) \\ \tilde{m}(2; p)/2 \\ \tilde{m}(-2; p)/2 \end{pmatrix}, \quad (34)$$

$$= \left(\sum_k \sum_{t \in p} A_{p,t}^{(k)\dagger} w_k f_{k,t} A_{t,p}^{(k)} \right)^{-1} \left(\sum_j \sum_{t \in p} A_{p,t}^{(j)\dagger} w_j f_{j,t} d_{j,t} \right). \quad (35)$$

We have assumed here the pixels to be infinitely small, so that, starting with Eq. (28), the location of all samples in a pixel coincides with the pixel center. The effect of the pixel's finite size and the so-called sub-pixel effects will be considered in Section 3.5.

2.4. Measured power spectra

To compute the cross-power spectrum of any two spin v_1 and v_2 maps, we first project each polarized component v of $\tilde{\mathbf{m}}(p)$ on the appropriate spin weighted sets of spherical harmonics,

$${}_x \tilde{m}_{\ell' m'}(v) = \int d\mathbf{r} \tilde{m}(v; \mathbf{r}) {}_x Y_{\ell' m'}^*(\mathbf{r}), \quad (36)$$

and average these terms according to

$$\tilde{C}_{\ell'}^{v_1 v_2} \equiv \frac{1}{2\ell' + 1} \sum_{m'} \langle v_1 \tilde{m}_{\ell' m'}(v_1) v_2 \tilde{m}_{\ell' m'}^*(v_2) \rangle, \quad (37)$$

$$= \sum_{u_1 u_2 j_1 j_2 \ell_s \ell_{s_2}} (-1)^{s_1 + s_2 + v_1 + v_2} C_{\ell}^{u_1 u_2} \frac{2\ell + 1}{4\pi} u_1 \hat{b}_{\ell_s}^{(j_1)*} u_2 \hat{b}_{\ell_{s_2}}^{(j_2)} \\ \times \frac{k_{u_1} k_{u_2}}{k_{v_1} k_{v_2}} \sum_{\ell' m'} \rho_{j_1, v_1} \rho_{j_2, v_2} \tilde{\omega}_{\ell' m'}^{(j_1)} \tilde{\omega}_{\ell' m'}^{(j_2)*} \begin{pmatrix} \ell & \ell' & \ell'' \\ -s_1 & s_1 + v_1 & -v_1 \end{pmatrix} \begin{pmatrix} \ell & \ell' & \ell'' \\ -s_2 & s_2 + v_2 & -v_2 \end{pmatrix}, \quad (38)$$

where Eq. (C.6) was used. The detailed derivation of this relation and its associated terms is given in Appendix A. Suffice it to say here that k_u terms are either 1 or 1/2, $u \hat{b}_{\ell_s}^{(j)}$ terms are inverse noise-weighted beam multipoles, and $\tilde{\omega}^{(j)}$ terms are effective weights describing the scanning and depending on the direction of polarization, hit redundancy (both from sky coverage and flagged samples), and noise level of detector j .

Equation (38) is therefore a generalization to non-circular beams of the pseudo-power spectra measured on a masked or weighted map (Hivon et al. 2002; Hansen & Górski 2003), and extends to polarization the Quickbeam non-circular beam formalism used in the data analysis conducted by Planck 2013-VII (2014). It also formally agrees with Hu et al. (2003)'s results on the impact of systematic effects on the polarization power spectra, with the functions $u \hat{b}_{\ell_s}^{(j)*} \rho_{j, v} \tilde{\omega}_{\ell' m'}^{(j)}$ absorbing the systematic effect parameters relative to detector j . In the next sections, we present the numerical results implied by this result and compare them on full-fledged Planck-HFI simulations.

3. Results

We now apply the QuickPol formalism to configurations representative of current or forthcoming CMB experiments, and to a couple of idealized test cases for which the expected result is already known, as a sanity check. The effect of the finite pixel size is also studied.

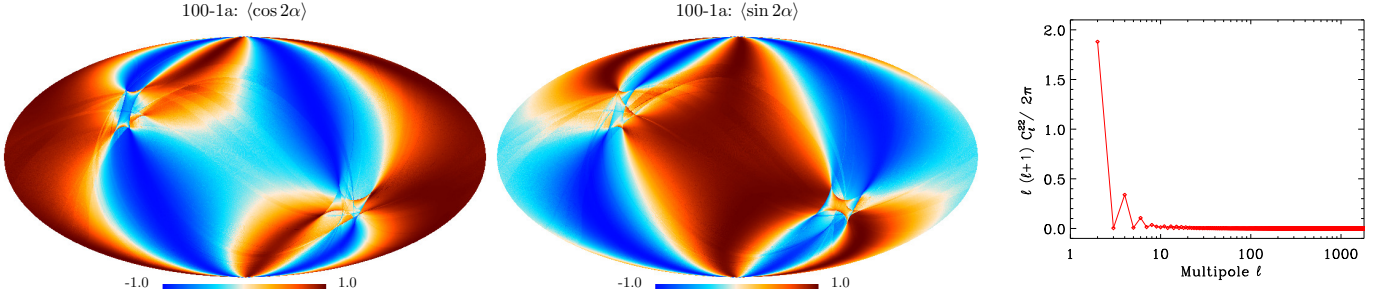


Fig. 1. Orientation of polarization measurements in *Planck*. The two left panels show, for an actual *Planck* detector, the maps of $\langle \cos 2\alpha \rangle$ and $\langle \sin 2\alpha \rangle$ respectively, where α is the direction of the polarizer with respect to the local Galactic meridian, which contributes to the spin 2 term $\omega_2^{(j)}$ defined in Eq. (A.3). The right panel shows the power spectrum C_ℓ^{22} of $\langle e^{2i\alpha} \rangle = \omega_2^{(j)}/\omega_0^{(j)}$, multiplied by $\ell(\ell+1)/2\pi$.

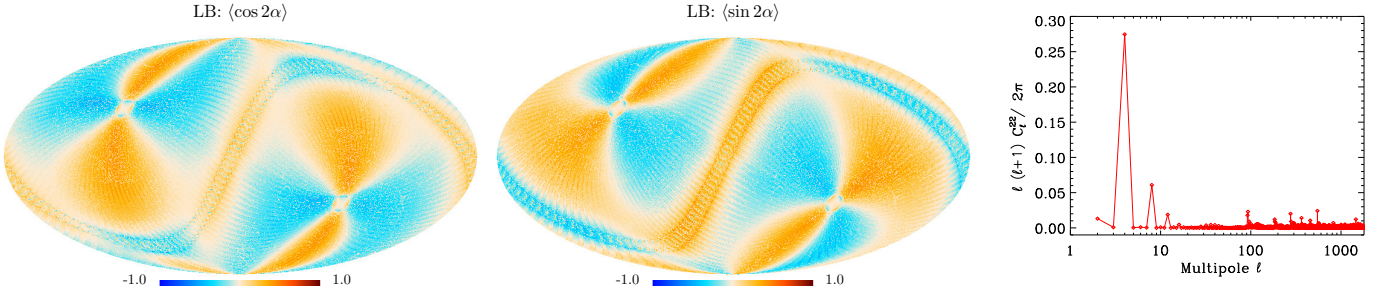


Fig. 2. Same as Fig. 1 for an hypothetical detector of a LiteBIRD-like mission, except for the right panel plot which has a different y-range.

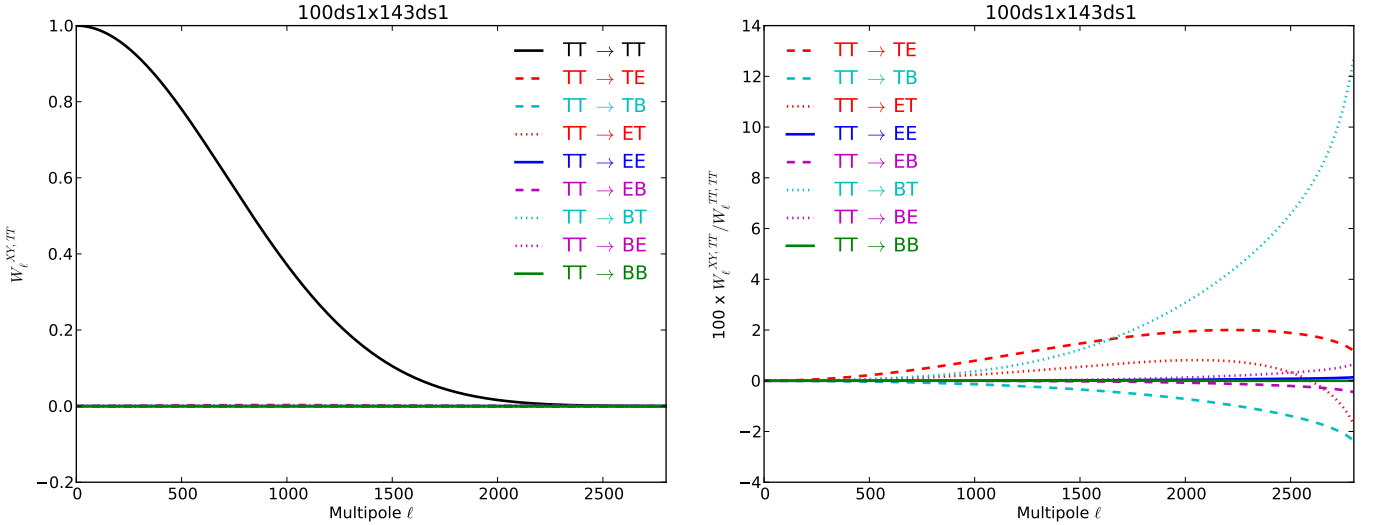


Fig. 3. Effective beam window matrix $W_\ell^{XY,TT}$ introduced in Eq. (41) and detailed in Eq. (E.8a), for the cross-spectra of two simulated *Planck* maps discussed in Section 5. Left panel: raw elements of $W_\ell^{XY,TT}$, showing for each ℓ how the measured XY map angular power spectrum is impacted by the input TT spectrum, because of the observation of the sky with the beams. Right panel: blown-up ratio of the non-diagonal elements to the diagonal ones: $100 W_\ell^{XY,TT}/W_\ell^{TT,TT}$.

3.1. A note about scanning strategies

To begin with, let us consider the scanning strategy of *Planck* and of another satellite mission optimized for the measurement of CMB polarization.

Figure 1 illustrates the orientation of the polarization measurements achieved in *Planck*. It shows, for an actual *Planck* detector, the maps of $\langle \cos 2\alpha \rangle$ and $\langle \sin 2\alpha \rangle$ respectively, where α is the direction of the polarizer with respect to the local Galactic meridian. These quantities contribute to the spin 2 term $\omega_2^{(j)}$ defined in Eq. (A.3). The large amplitude of these two maps is consistent with the fact that for a given detector, the orientation of the polarization measurements is mostly α and $-\alpha$, as expected when detectors move

on almost great circles with very little precession. Another striking feature is the relative smoothness of the maps, which translate into the power spectrum C_ℓ^{22} of $\langle e^{2i\alpha} \rangle = \omega_2^{(j)}/\omega_0^{(j)}$ peaking at low ℓ values.

Figure 2 shows the same information for an hypothetical LiteBIRD⁵ like detector (but *without* half-wave plate modulation) in which we assumed the detector to cover a circle of 45° in radius in one minute, with its spin axis precessing with a period of four days at 50° from the anti-sun direction. As expected for such a scanning strategy, the values of α are pretty uniformly distributed over the range $[0, 2\pi]$, which translates into a low amplitude of the $\langle \cos 2\alpha \rangle$ and $\langle \sin 2\alpha \rangle$ maps. Even if those maps do not look as smooth as those of *Planck*, their power spectra peak at fairly low multipole values.

3.2. Arbitrary beams, smooth scanning case

If one assumes that $\omega_s(p)$ and $\bar{\omega}_s(p)$ vary slowly across the sky, as we just saw in the case of *Planck* and LiteBIRD - and probably a wider class of orbital and sub-orbital missions - then ${}_s\bar{\omega}_{\ell'm'}$ is dominated by low ℓ' values and one expects $\ell \simeq \ell'$ because of the triangle relation imposed by the 3J symbols (see Appendix C). If one further assumes C_ℓ and b_ℓ to vary slowly in ℓ , then Eqs. (C.5) and (C.9) can be used to impose $s_1 + v_1 = s_2 + v_2 = s$ in Eq. (38) and provide

$$\bar{C}_\ell^{v_1 v_2} = \sum_{u_1 u_2} C_\ell^{u_1 u_2} \frac{k_{u_1} k_{u_2}}{k_{v_1} k_{v_2}} \sum_{j_1 j_2} \sum_s u_1 \hat{b}_{\ell, s-v_1}^{(j_1)*} u_2 \hat{b}_{\ell, s-v_2}^{(j_2)} \bar{\Omega}_{v_1, v_2, s}^{(j_1 j_2)}, \quad (39)$$

with

$$\bar{\Omega}_{v_1, v_2, s}^{(j_1 j_2)} \equiv \rho_{j_1, v_1} \rho_{j_2, v_2} \frac{1}{4\pi} \sum_{\ell' m'} {}_s\bar{\omega}_{\ell' m'}^{(j_1)} [v_1] {}_s\bar{\omega}_{\ell' m'}^{(j_2)*} [v_2], \quad (40a)$$

$$= \rho_{j_1, v_1} \rho_{j_2, v_2} \frac{1}{N_{\text{pix}}} \sum_p \bar{\omega}_s^{(j_1)} [v_1](p) \bar{\omega}_s^{(j_2)*} [v_2](p), \quad (40b)$$

$$= \bar{\Omega}_{-v_1, -v_2, -s}^{(j_1 j_2)*}. \quad (40c)$$

As derived in Appendix E.1, Eq. (39) reduces to a mixing equation relating the observed cross-power spectra to the true ones:

$$\bar{C}_\ell^{XY} = \sum_{X' Y'} W_\ell^{XY, X' Y'} C_\ell^{X' Y'} \quad (41)$$

with $X, Y, X', Y' \in \{T, E, B\}$.

In the smooth scanning case representative of past and forthcoming satellite missions, the effect of observing the sky with non-ideal beams is therefore to couple the temperature and polarization power spectra $C_\ell^{X' Y'}$ at the same multipole ℓ through an extended beam window matrix $W_\ell^{XY, X' Y'}$, as illustrated on Fig. 3.

3.3. Arbitrary scanning, circular identical beams

If the scanning beams are now assumed to all be circular and identical, the measured $\bar{C}(\ell)$ will not depend on the details of the scanning strategy, orientation of the detectors, or relative weights of the detectors. We are indeed exactly in the ideal hypotheses of the map making formalism (Eq. 29) and get the well known and simple result that the effect of the beam can be factored out.

If one considers detectors with identical circular copolarized beams, and whose actual polarization efficiency was used during the map making: $\rho_j = \rho'_j$, such that

$${}_u \hat{b}_{\ell, s}^{(j)} \equiv w_j q_\ell {}_u b_{\ell, s}^{(j)} = w_j q_\ell \rho_{ju} b_\ell \delta_{s, -u}, \quad (42)$$

then Eqs. (39) and (40b) feature terms like $\sum_j {}_u \hat{b}_{\ell, s-v}^{(j)*} \rho_{jv} \bar{\omega}_s^{(j)} [v]$, which when written in a matrix form, verify the equality

$$q_\ell b_\ell \sum_j w_j \begin{pmatrix} \bar{\omega}_0^{(j)} [0] & \rho_j \bar{\omega}_{-2}^{(j)} [0] & \rho_j \bar{\omega}_2^{(j)} [0] \\ \rho_j \bar{\omega}_2^{(j)} [2] & \rho_j^2 \bar{\omega}_0^{(j)} [2] & \rho_j^2 \bar{\omega}_4^{(j)} [2] \\ \rho_j \bar{\omega}_{-2}^{(j)} [-2] & \rho_j^2 \bar{\omega}_{-4}^{(j)} [-2] & \rho_j^2 \bar{\omega}_0^{(j)} [-2] \end{pmatrix} = q_\ell b_\ell \begin{pmatrix} 1 & 0 & 0 \\ 0 & 1 & 0 \\ 0 & 0 & 1 \end{pmatrix}, \quad (43)$$

according to Eq. (B.9). The measured power spectra are then

$$\bar{C}_\ell^{XY} = \hat{b}_\ell^2 C_\ell^{XY} = q_\ell^2 b_\ell^2 C_\ell^{XY}, \quad (44)$$

and $\bar{C}_\ell^{XY} = \exp(-\ell(\ell+1)\sigma^2) C_\ell^{XY}$ for the Gaussian circular beam introduced in Eq. (23a). Obviously, these very simple results assume that the whole sky is observed. If not, the cut-sky induced $\ell - \ell$ and $E - B$ coupling effects mentioned at the end of Section 2.4 have to be accounted for, as described, for example, in Chon et al. (2004), Mitra et al. (2009), Grain et al. (2009), and references therein.

⁵ <http://litebird.jp/eng/>.

3.4. Arbitrary beams, ideal scanning

Let us now consider the case of an ideal scanning of the sky, for which in any pixel p , the number of valid (unflagged) samples is the same for all detectors $h_j(p) = h(p)$, and each detector j covers uniformly all possible orientations within that pixel along the duration of the mission. This constitutes the ideal limit aimed at by the scanning strategy illustrated in Fig. 2. The assumption of smooth scanning is then perfectly valid, and details of the calculations can be found in Appendix E.2. We find for instance that the matrix describing how the measured temperature and polarization power spectra are affected by the input TT spectrum reads

$$W_\ell^{XY, TT} \equiv \begin{pmatrix} W_\ell^{TT, TT} \\ W_\ell^{EE, TT} \\ W_\ell^{BB, TT} \\ W_\ell^{TE, TT} \\ W_\ell^{TB, TT} \\ W_\ell^{EB, TT} \\ W_\ell^{ET, TT} \\ W_\ell^{BT, TT} \\ W_\ell^{BE, TT} \end{pmatrix} = \sum_{j_1 j_2} \begin{pmatrix} \hat{b}_{\ell,0}^{(j_2)} \hat{b}_{\ell,0}^{(j_1)*} \xi_{00} \\ (\hat{b}_{\ell,-2}^{(j_2)} + \hat{b}_{\ell,2}^{(j_2)}) (\hat{b}_{\ell,-2}^{(j_1)*} + \hat{b}_{\ell,2}^{(j_1)*}) \rho_{j_1} \rho_{j_2} \xi_{22} \\ (\hat{b}_{\ell,-2}^{(j_2)} - \hat{b}_{\ell,2}^{(j_2)}) (\hat{b}_{\ell,-2}^{(j_1)*} - \hat{b}_{\ell,2}^{(j_1)*}) \rho_{j_1} \rho_{j_2} \xi_{22} \\ -(\hat{b}_{\ell,-2}^{(j_2)} + \hat{b}_{\ell,2}^{(j_2)}) \hat{b}_{\ell,0}^{(j_1)*} \rho_{j_2} \xi_{02} \\ -i(\hat{b}_{\ell,-2}^{(j_2)} - \hat{b}_{\ell,2}^{(j_2)}) \hat{b}_{\ell,0}^{(j_1)*} \rho_{j_2} \xi_{02} \\ i(\hat{b}_{\ell,-2}^{(j_2)} - \hat{b}_{\ell,2}^{(j_2)}) (\hat{b}_{\ell,-2}^{(j_1)*} + \hat{b}_{\ell,2}^{(j_1)*}) \rho_{j_1} \rho_{j_2} \xi_{22} \\ -\hat{b}_{\ell,0}^{(j_2)} (\hat{b}_{\ell,-2}^{(j_1)*} + \hat{b}_{\ell,2}^{(j_1)*}) \rho_{j_1} \xi_{20} \\ i\hat{b}_{\ell,0}^{(j_2)} (\hat{b}_{\ell,-2}^{(j_1)*} - \hat{b}_{\ell,2}^{(j_1)*}) \rho_{j_1} \xi_{20} \\ -i(\hat{b}_{\ell,-2}^{(j_2)} + \hat{b}_{\ell,2}^{(j_2)}) (\hat{b}_{\ell,-2}^{(j_1)*} - \hat{b}_{\ell,2}^{(j_1)*}) \rho_{j_1} \rho_{j_2} \xi_{22} \end{pmatrix}, \quad (45)$$

with the normalization factors

$$\xi_{00}^{-1} = \sum_{k_1 k_2} w_{k_1} w_{k_2}, \quad \xi_{02}^{-1} = \sum_{k_1 k_2} w_{k_1} w_{k_2} \rho_{k_2}^2, \quad \xi_{20}^{-1} = \sum_{k_1 k_2} w_{k_1} w_{k_2} \rho_{k_1}^2, \quad \xi_{22}^{-1} = \sum_{k_1 k_2} w_{k_1} w_{k_2} \rho_{k_1}^2 \rho_{k_2}^2. \quad (46)$$

This confirms that in this ideal case, as expected and discussed previously (e.g., Wallis et al. 2014, and references therein), the leakage from temperature to polarization (Eq. 45) is driven by the beam ellipticity ($\hat{b}_{\ell,\pm 2}^{(j)}$ terms) which has the same spin ± 2 as polarization. One also sees that the contamination of the E and B spectra by T are swapped (e.g., $W_\ell^{EE, TT} \longleftrightarrow W_\ell^{BB, TT}$) when the beams are rotated with respect to the polarimeter direction by 45° ($\hat{b}_{\ell,\pm 2} \longrightarrow \pm i\hat{b}_{\ell,\pm 2}$), as shown in Shimon et al. (2008).

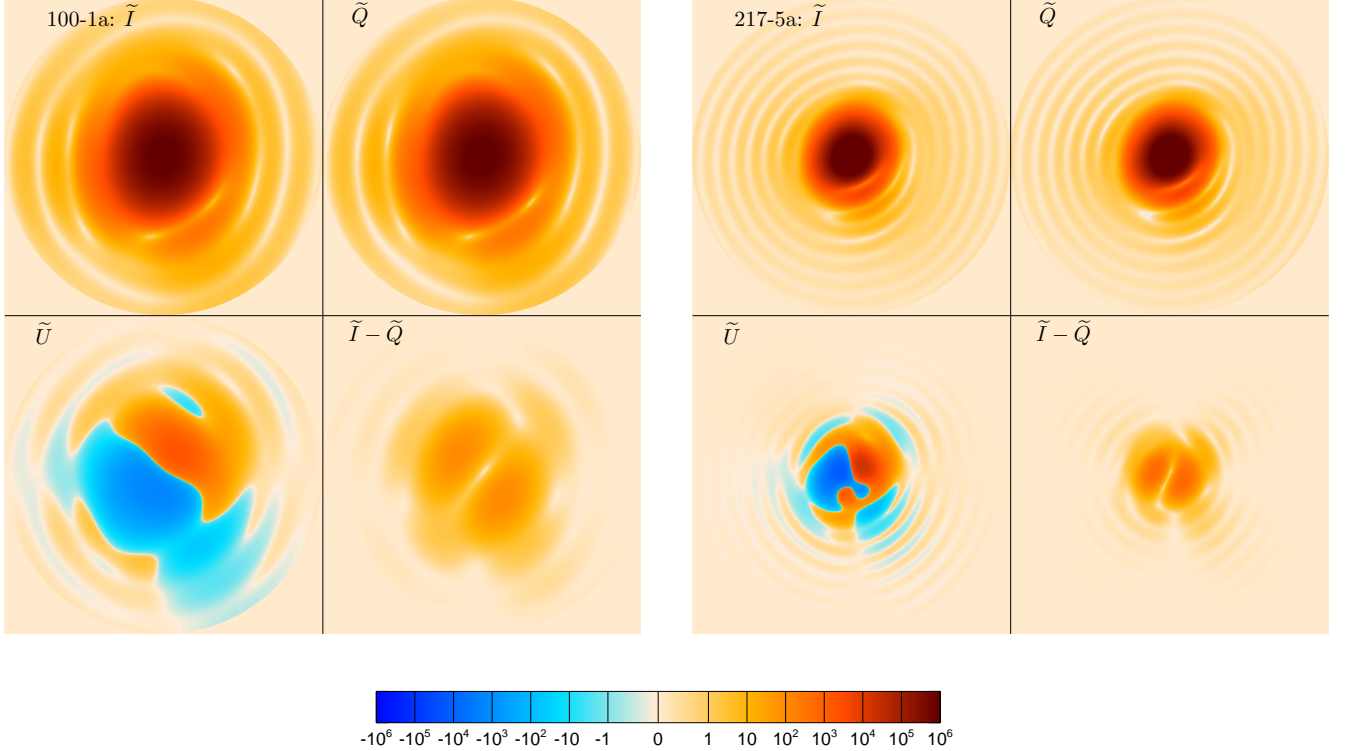


Fig. 4. Computer simulated beam maps (\tilde{I} , \tilde{Q} , $\tilde{I} - \tilde{Q}$ and \tilde{U} clockwise from top-left) for two of the *Planck*-HFI detectors (100-1a and 217-5a) used in the validation of QuickPol. Each panel is $1^\circ \times 1^\circ$ in size, and the units are arbitrary.

3.5. Finite pixel size and sub-pixel effects

As shown in [Planck 2013-VII \(2014\)](#), in the case of temperature fluctuations, the effect of the finite pixel size is twofold. First, in each pixel, the distance between the nominal pixel center and the center of mass of the observations couples to the local gradient of the Stokes parameters to induce noise terms. Second, there is a smearing effect due to the integration of the signal over the surface of the pixel. Equation (41) then becomes

$$\widetilde{C}_\ell^{XY} = W_\ell^{\text{pix}} \sum_{X'Y'} W_\ell^{XY, X'Y'} C_\ell^{X'Y'} + N_\ell^{XY} \quad (47)$$

with $W_\ell^{\text{pix}} = 1 - \ell(\ell + 1)\sigma^2/2 + \mathcal{O}((\sigma\ell)^3)$, and $\sigma^2 = \langle \text{dr}^2 \rangle$ the squared displacement averaged over the hits in the pixels and over the set of considered pixels. As shown in [Appendix F](#), the additive noise term, sourced by the temperature gradient within the pixel, affects both temperature and polarization measurements, with $N_\ell^{EE} = N_\ell^{BB}$ and $|N_\ell^{EE}| \lesssim |N_\ell^{TT}|$, while the other spectra are much less affected, that is, $|N_\ell^{TE}|, |N_\ell^{TB}|, |N_\ell^{EB}| \ll |N_\ell^{TT}|$. The sign of this noise term is arbitrary and can be negative when cross-correlating maps with a different sampling of the pixels.

4. Numerical implementation

Numerical implementations of this formalism are performed in three steps, assuming that the individual beam $b_{\ell s}^{(j)}$ is already computed for $0 \leq s \leq s_{\text{max}} + 4$ and $0 \leq \ell \leq \ell_{\text{max}}$:

1. For each involved detector j , and for $0 \leq s \leq s_{\text{max}}$, one computes the s -th complex moment of its direction of polarization in pixel p : $\omega_s^{(j)}(p)$ defined in Eq. (A.3). Since this requires processing the whole scanning data stream, this step can be time consuming. However it has to be computed only once for all cases, independently of the choices made elsewhere on the beam models, calibrations, noise weighting, and other factors. As we shall see below, it may not even be necessary to compute it, or store it, for every sky pixel.
2. The $\omega_s^{(j)}(p)$ computed above are weighted with the assumed inverse noise variance weights w_j and polar efficiencies ρ_j to build the hit matrix \mathbf{H} in each pixel, which is then inverted to compute the $\widetilde{\omega}_s^{(j)}(p)$, defined in Eq. (A.6). Those are then multiplied together to build the scanning information matrix $\widetilde{\Omega}$ using its pixel space definition (Eq. 40b). The resulting complex matrix contains $9n_1n_2(2s_{\text{max}} + 1)$ elements, where n_1 and n_2 are the number of detectors in each of the two detector assemblies whose cross-spectra are considered. This step can be parallelized to a large extent, and can be dramatically sped up by building this matrix out of a representative subset of pixels. In our comparison to simulations, described in [Section 5](#), and performed on HEALPix map with $n_{\text{side}} = 2048$ and $N_{\text{pix}} = 12n_{\text{side}}^2 = 50 \cdot 10^6$ pixels, we checked that using only $N_{\text{pix}}/64$ pixels evenly spread on the sky gave final results almost identical to those of the full calculations.
3. Finally, using Eqs. (E.1-41) we note that $W_\ell^{XY, X'Y'} = \partial \widetilde{C}_\ell^{XY} / \partial C_\ell^{X'Y'}$, so that, for instance, for a given ℓ , the 3×3 $W_\ell^{XY, TE}$ matrix is computed by replacing in Eq. (E.1) its central term C_ℓ with its partial derivative, such as

$$\frac{\partial}{\partial C_\ell^{TE}} C_\ell = \mathbf{R}_2 \cdot \frac{\partial}{\partial C_\ell^{TE}} \begin{pmatrix} C_\ell^{TT} & C_\ell^{TE} & C_\ell^{TB} \\ C_\ell^{ET} & C_\ell^{EE} & C_\ell^{EB} \\ C_\ell^{BT} & C_\ell^{BE} & C_\ell^{BB} \end{pmatrix} \cdot \mathbf{R}_2^\dagger \quad (48)$$

$$= \mathbf{R}_2 \cdot \begin{pmatrix} 0 & 1 & 0 \\ 1 & 0 & 0 \\ 0 & 0 & 0 \end{pmatrix} \cdot \mathbf{R}_2^\dagger, \quad (49)$$

where we assumed in Eq. (49) that, on the sky, $C_\ell^{TE} = C_\ell^{ET}$ and generally $C_\ell^{X'Y'} = C_\ell^{Y'X'}$, like for CMB anisotropies.

On the other hand, when dealing with arbitrary foregrounds cross-frequency spectra, we would have to assume $C_\ell^{X'Y'} \neq C_\ell^{Y'X'}$ when $X' \neq Y'$, and compute $W_\ell^{XY, X'Y'}$ and $W_\ell^{XY, Y'X'}$ separately. As we shall see in [Section 6](#), this final and fastest step is the only one that needs to be repeated in a Monte-Carlo analysis of instrumental errors, and it can be sped up. Indeed, since the input $b_{\ell m}$ and output W_ℓ are generally very smooth functions of ℓ , it is not necessary to do this calculation for every single ℓ , but rather for a sparse subset of them, for instance regularly interspaced by $\delta\ell$. The resulting W_ℓ matrix is then B-spline interpolated. In our test cases with $\theta_{\text{FWHM}} = 10$ to $5'$, using $\delta\ell = 10$ leads to relative errors on the final product below 10^{-5} for each ℓ .

In our tests, with $s_{\text{max}} = 6$, $\ell_{\text{max}} = 4000$, $n_1 = n_2 = 4$, and all proposed speed-ups in place, Step 2 took about ten minutes, dominated by IO, while Step 3 took less than a minute on one core of a 3GHz Intel Xeon CPU. The final product is a set of six (or nine) real matrices $W_\ell^{XY, X'Y'}$, each with $9(\ell_{\text{max}} + 1)$ elements.

5. Comparison to Planck-HFI simulations

The differential nature of the polarization measurements, in the absence of modulating devices such as rotating half-wave plates, means that any mismatch between the responses of the two (or more) detectors being used will leak a fraction of temperature into polarization. This was observed in *Planck*, even though pairs of polarized orthogonal detectors observed the sky through the same horn, therefore with almost identical optical beams. Optical mismatches within pairs of detectors were enhanced by residuals of the electronic time response deconvolution which could affect their respective scanning beams differently ([Planck 2013-IV 2014](#);

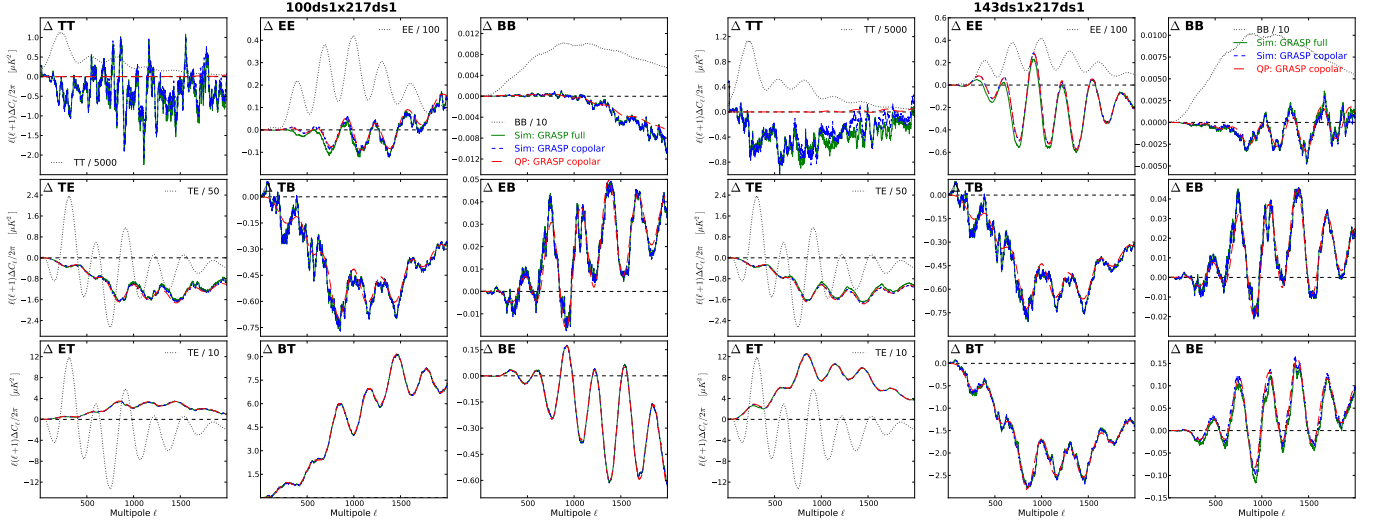


Fig. 5. Comparison to simulations for 100ds1x217ds1 (lhs panels) and 143ds1x217ds1 (rhs panels) cross power spectra, for computer simulated beams. In each panel is shown the discrepancy between the actual $\ell(\ell + 1)C_\ell/2\pi$ and the one in input, smoothed on $\Delta\ell = 31$. Results obtained on simulations with either the full beam model (green curves) or the co-polarized beam model (blue dashes) are to be compared to QuickPol analytical results (red long dashes). In panels where it does not vanish, a small fraction of the input power spectrum is also shown as black dots for comparison.

Planck 2013-VII 2014). Other sources of mismatch included their different noise levels and thus their respective statistical weight on the maps, which could reach relative differences of up to 80%, and the number of valid samples which could vary by up to 20% between detectors. As seen previously, these detector-specific features can be included in the QuickPol pipeline in order to describe as closely as possible the actual instrument. In this section, we show how we actually did it and how QuickPol compares to full-fledged simulations of *Planck*-HFI observations.

Noiseless simulations of *Planck*-HFI observations of a pure CMB sky were run for quadruplets of polarized detectors at three different frequencies (100, 143, and 217GHz), and identified as 100ds1, 143ds1, and 217ds1 respectively. The input CMB power spectrum C_ℓ^{XY} was assumed to contain no primordial tensorial modes, with the traditional $C_\ell^{TB} = C_\ell^{EB} = 0$ and $C_\ell^{XY} = C_\ell^{YX}$. The same mission duration, pointing, polarization orientations (γ_j) and efficiencies (ρ_j), flagged samples, and discarded pointing periods (f_j) were used as in the actual observations, with computer simulated polarized optical beams for the relevant detectors produced with the GRASP⁶ physical optics code (Rosset et al. 2007, and references therein) as illustrated on Fig. 4. Data streams were generated with the LevelS simulation pipeline (Reinecke et al. 2006), using the Conviqt code (Prézeau & Reinecke 2010) to perform the convolution of the sky with the beams, including the $b_{\ell s}$ for $|s| \leq s_{\max} = 14$ and $\ell \leq \ell_{\max} = 4800$. Polarized maps of each detector set were produced with the Polkapix destriping code (Tristram et al. 2011), assuming the same noise-based relative weights (w_j) as the actual data, and their cross spectra were computed over the whole sky with HEALPix anafast routine to produce the empirical power spectra \hat{C}_ℓ^{XY} .

The same exercise was reproduced replacing the initial $\tilde{I}, \tilde{Q}, \tilde{U}$ beam maps with a purely co-polarized beam based on the same \tilde{I} , in order to test the validity of the co-polarized assumption in *Planck*.

Figure 5 shows how the empirical power spectra are different from the input ones,

$$\Delta\hat{C}_\ell^{XY} = \frac{\hat{C}_\ell^{XY}}{W_\ell^{\text{pix}} W_\ell^{XY, XY}} - C_\ell^{XY}, \quad (50)$$

after correction from the pixel and (scalar) beam window functions, and compares those to the QuickPol predictions

$$\Delta\tilde{C}_\ell^{XY} = \frac{W_\ell^{\text{pix}} \sum_{X'Y'} W_\ell^{XY, X'Y'} C_\ell^{X'Y'}}{W_\ell^{\text{pix}} W_\ell^{XY, XY}} - C_\ell^{XY}, \quad (51)$$

for all nine possible values of XY for the cross-spectra of detector sets 100ds1x217ds1 and 143ds1x217ds1. The results are actually multiplied by the usual $\ell(\ell + 1)/2\pi$ factor, and smoothed on $\Delta\ell = 31$. The empirical results are shown both for the full-fledged beam model (green curves) and the purely co-polarized model (blue dashes). One sees that the change, mostly visible in the EE case, is very small, validating the co-polarized beam assumption, at least within the limits of this computer simulated *Planck* optics. The QuickPol predictions, only shown in the co-polarized case for clarity (long red dashes), agree extremely well with the corresponding numerical simulations. We have checked that this agreement to simulations remains true in the full beam model.

⁶ TICRA: <http://www.ticra.com>.

6. Propagation of instrumental uncertainties

We assumed so far the instrument to be non-ideal, but exactly known. In practice, however, the instrument is only known with limited accuracy and the final beam matrix will be affected by at least four types of uncertainties:

- limited knowledge of the beam angular response, which affects the $b_{\ell m}^{(j)}$, replacing them with $b_{\ell m}^{\prime(j)}$ while preserving the beam total throughput after calibration (see below) $b_{00}^{\prime(j)} = b_{00}^{(j)}$. We therefore assume the beam power spectrum $W_\ell = \sum_m |b_{\ell m}|^2 / (2\ell + 1)$ to be the same at $\ell = 0$, where the beam throughput is defined, and at $\ell = 1$, where the detector gain calibration is usually done using the CMB dipole.
- error on the gain calibration of detector j , which translates into $b_{\ell m}^{(j)} \rightarrow (1 + \delta c_j) b_{\ell m}^{(j)}$, with $|\delta c_j| \ll 1$,
- error on the polar efficiency of detector j , which translates into $\rho_j' = \rho_j(1 + \delta\rho_j/\rho_j)$. As discussed in Section 2.1, we expect in the case of *Planck*-HFI a relative uncertainty $|\delta\rho_j/\rho_j| < 1\%$.
- error on the actual direction of polarization: for each detector j , the direction of polarization measured in a common referential becomes $\gamma_j \rightarrow \gamma_j + \delta\gamma_j$. In the case of *Planck*-HFI, Rosset et al. (2010) found the pre-flight measurement of this angle to be dominated by systematic errors of the order of 1° for polarization sensitive bolometers (PSBs). These uncertainties can be larger for spider web bolometers (SWBs), but as we shall see below, the coupling with the low polarization efficiency ρ_j of those detectors makes them somewhat irrelevant.

All these uncertainties can be inserted in Eq. (E.1) by substituting Eq. (E.4)

$$\hat{\mathbf{B}}_{\ell,s}^{(j)} = \begin{pmatrix} \hat{b}_{\ell,s}^{(j)} & \hat{b}_{\ell,s-2}^{(j)} & \hat{b}_{\ell,s+2}^{(j)} \\ \rho_j \hat{b}_{\ell,s+2}^{(j)} & \rho_j \hat{b}_{\ell,s}^{(j)} & \rho_j \hat{b}_{\ell,s+4}^{(j)} \\ \rho_j \hat{b}_{\ell,s-2}^{(j)} & \rho_j \hat{b}_{\ell,s-4}^{(j)} & \rho_j \hat{b}_{\ell,s}^{(j)} \end{pmatrix},$$

with

$$\hat{\mathbf{B}}_{\ell,s}^{\prime(j)} = (1 + \delta c_j) \begin{pmatrix} 1 & 0 & 0 \\ 0 & \rho_j x_j & 0 \\ 0 & 0 & \rho_j x_j^* \end{pmatrix} \cdot \begin{pmatrix} \hat{b}_{\ell,s}^{\prime(j)} & \hat{b}_{\ell,s-2}^{\prime(j)} & \hat{b}_{\ell,s+2}^{\prime(j)} \\ \hat{b}_{\ell,s+2}^{\prime(j)} & \hat{b}_{\ell,s}^{\prime(j)} & \hat{b}_{\ell,s+4}^{\prime(j)} \\ \hat{b}_{\ell,s-2}^{\prime(j)} & \hat{b}_{\ell,s-4}^{\prime(j)} & \hat{b}_{\ell,s}^{\prime(j)} \end{pmatrix}, \quad (52)$$

where $x_j = (1 + \delta\rho_j/\rho_j)e^{2i\delta\gamma_j}$.

As mentioned in Section 3, such substitutions are done in Step 3 of the QuickPol pipeline. A new set of numerical values for the instrument model can therefore be turned rapidly into a beam window matrix (Eq. 41), allowing, for instance, a Monte-Carlo exploration at the power spectrum level of the instrumental uncertainties.

7. About rotating half-wave plates

In the previous sections we have focused on experiments that rely on the rotation of the full instrument with respect to the sky to have the angular redundancy required to measure the Stokes parameters. An alternative way is to rotate the incoming polarization at the entrance of the instrument while leaving the rest fixed. This is most conveniently achieved with a rotating half-wave plate (rHWP). The rotation is either stepped (Polarbear Collaboration: Ade et al. 2014) or continuous (Chapman et al. 2014; Essinger-Hileman et al. 2016; Ritacco et al. 2016a). The advantages of this system are numerous, the first of which is the decoupling between the optimization of the scanning strategy in terms of “pure” redundancy and its optimization in terms of “angular” redundancy. It is much easier to control the rotation of a rHWP than of a full instrument and therefore ensure an optimal angular coverage whatever the observation scene is. If the rotation is continuous and fast, typically of the order of 1 Hz, it has the extra advantage of modulating polarization at frequencies larger than the atmospheric and electronics $1/f$ noise knee frequency, hence ensuring a natural rejection of these low frequency noises. Furthermore, this allows us to build I , Q , and U maps per detector, without needing to combine different detectors with their associated bandpass mismatch or other differential systematic effects mentioned in the previous sections. Individual detector systematics therefore tend to average out rather than combine to induce leakage between sky components. On the down side, this comes at the price of moving a piece of hardware in the instrument and all its associated systematic effects, starting with a signal that is synchronous with the rHWP rotation as observed in Johnson et al. (2007), Chapman et al. (2014), and Ritacco et al. (2016b).

Such trade-offs are being investigated by current experiments using rHWPs and will certainly be studied in more details in preparation of future CMB orbital and sub-orbital missions, such as CMB-S4 network (CMB-S4 collaboration 2016). We here briefly comment on how the addition of a rHWP to an instrument can be coped with in QuickPol.

The Jones matrix of a HWP (which shifts the y -axis electric field by a half period) rotated by an angle ψ is (O’Dea et al. 2007)

$$\mathbf{J}_{\text{rHWP}}(\psi) = \mathbf{R}_\psi \cdot \begin{pmatrix} 1 & 0 \\ 0 & -1 \end{pmatrix} \cdot \mathbf{R}_\psi^\dagger, \quad (53)$$

$$= \begin{pmatrix} \cos 2\psi & \sin 2\psi \\ \sin 2\psi & -\cos 2\psi \end{pmatrix}. \quad (54)$$

If a rotating HWP is installed at the entrance of the optical system, the Jones matrix of the system becomes $\mathbf{J}(\mathbf{r}_\alpha) \rightarrow \mathbf{J}(\mathbf{r}_\alpha, \psi) = \mathbf{J}(\mathbf{r}_\alpha) \mathbf{J}_{\text{rHWP}}(\psi)$, and the signal observed in the presence of arbitrary beams (Eq. 8) becomes (after dropping the circular polarization

V terms)

$$d(\alpha, \psi) = \frac{1}{2} \int d\mathbf{r} \left[\tilde{T}(\alpha, \psi, \mathbf{r}) T(\mathbf{r}) + \tilde{Q}(\alpha, \psi, \mathbf{r}) Q(\mathbf{r}) + \tilde{U}(\alpha, \psi, \mathbf{r}) U(\mathbf{r}) \right], \quad (55)$$

with

$$\tilde{T}(\alpha, \psi, \mathbf{r}) = \tilde{T}(\mathbf{r}_\alpha), \quad (56a)$$

$$\tilde{Q}(\alpha, \psi, \mathbf{r}) = \tilde{Q}(\mathbf{r}_\alpha) \cos(2\alpha + 4\psi) + \tilde{U}(\mathbf{r}_\alpha) \sin(2\alpha + 4\psi), \quad (56b)$$

$$\tilde{U}(\alpha, \psi, \mathbf{r}) = \tilde{Q}(\mathbf{r}_\alpha) \sin(2\alpha + 4\psi) - \tilde{U}(\mathbf{r}_\alpha) \cos(2\alpha + 4\psi). \quad (56c)$$

These new beams can then be passed to Eq. (30) and propagated through the rest of QuickPol. Together with Eq. (9), we see that, if ψ is correctly chosen, the modulation of Q and U , by $2\alpha + 4\psi$, is now clearly different from that of T which depends only on α via \mathbf{r}_α , even for non-circular \tilde{T} beams. The leakages from temperature to polarization are therefore expected to be much smaller than when the polarization modulation is performed only by a rotation of the whole instrument, and O’Dea et al. (2007) showed, that even for non-ideal rHWP, the induced systematic effects are limited to polarization cross-talks without temperature to polarization leakage.

As previously mentioned, specific systematic effects such as the rotation synchronous signal must be treated with care. Once such time domain systematic effects are identified and modeled, they, together with realistic optical properties of the instrument, can be integrated in the QuickPol formalism in order to be taken into account, quantified, and/or marginalized over at the power spectrum level.

8. Conclusions

Polarization measurements are mostly obtained by differencing observations by different detectors. Mismatch in their optical beams, time responses, bandpasses, and so on induces systematic effects, for example, temperature to polarization leakage. The QuickPol formalism allows us to compute accurately and efficiently the induced cross-talk between temperature and polarization power spectra. It also provides a fast and easy way to propagate instrumental modeling uncertainties down to the final angular power spectra and is thus a powerful tool to simulate observations and to help with the design and specifications of future experiments, such as acceptable beam distortions, polarization modulation optimization, and observation redundancy. It can cope with time varying instrumental parameters, realistic sample flagging, and rejection. The method was validated through comparison to numerical simulations of realistic *Planck* observations. The hypotheses required on the instrument and survey, described in Sections 2 and 3, are extremely general and apply to *Planck* and to forthcoming CMB experiments such as PIXIE, LiteBIRD, CORe, and others. Contrary to Monte-Carlo based methods, such as FEBECoP, the impact of the beam related imperfections on the measured power spectra are obtained without having to assume any prior knowledge of the sky power spectra.

Of course, the beam matrices provided by QuickPol can be used in the cosmological analysis of a CMB survey. Indeed, the sky power spectra can be modeled as functions of cosmological parameters $\{\theta_C\}$, foreground modeling $\{\theta_F\}$, and nuisance parameters $\{\theta_n\}$. These $C_\ell^{XY}(\{\theta_C\}, \{\theta_F\}, \{\theta_n\})$ can then be generated, multiplied with the beam matrices $W_\ell^{X'Y', XY}$ for the set of detectors being analyzed, and compared to the measured $\tilde{C}_\ell^{X'Y'}$ in a maximum likelihood sense, in the presence of instrumental noise. The parameters $\{\theta_C\}, \{\theta_F\}, \{\theta_n\}$ can be iterated or integrated upon, with statistical priors, until a posterior distribution is built. In this kind of forward approach, it is not necessary to correct the observations from possibly singular transfer functions, nor to back-propagate the noise. At least some of the instrumental uncertainties $\{\theta_I\}$ affecting the effective beam via $W_\ell^{X'Y', XY}(\{\theta_I\})$ could be included in the overall analysis, and marginalized over, thanks to the fast calculation times by QuickPol of the impact of changes in the gain calibrations, polarization angles, and efficiencies, as discussed in Section 6. While QuickPol has been originally developed and tested in the case of experiments without a rotating half-wave plate, it is straightforward to add one to the current pipeline and assess its impact on the aforementioned systematics. Specific additional effects such as a HWP rotation synchronous signal or the effect of a tilted HWP are expected to show up in real experiments. As long as these can be physically modeled, they can be inserted in QuickPol as well.

Acknowledgements. Thank you to the *Planck* collaboration, and in particular to D. Hanson, K. Benabed, and F. R. Bouchet for fruitful discussions. Some results presented here were obtained with the HEALPix library.

References

- Armitage-Caplan, C. & Wandelt, B. D., PReBeaM for Planck: A Polarized Regularized Beam Deconvolution Map-Making Method. 2009, ApJS, 181, 533, [arXiv:0807.4179 1](#)
- Bennett, C. L., Larson, D., Weiland, J. L., et al., Nine-year Wilkinson Microwave Anisotropy Probe (WMAP) Observations: Final Maps and Results. 2013, ApJS, 208, 20, [arXiv:1212.5225v1 1](#)
- Bunn, E. F., Zaldarriaga, M., Tegmark, M., & de Oliveira-Costa, A., E/B decomposition of finite pixelized CMB maps. 2003, Phys. Rev. D, 67, 023501, [arXiv:astro-ph/0207338v1 F](#)
- Challinor, A., Fosalba, P., Mortlock, D., et al., All-sky convolution for polarimetry experiments. 2000, Phys. Rev. D, 62, 123002, [arXiv:astro-ph/0008228v2 2.2, 2.2](#)
- Chapman, D., Aboobaker, A. M., Ade, P., et al. 2014, in American Astronomical Society Meeting Abstracts, Vol. 223, American Astronomical Society Meeting Abstracts #223, 407.03 7
- Chon, G., Challinor, A., Prunet, S., Hivon, E., & Szapudi, I., Fast estimation of polarization power spectra using correlation functions. 2004, Monthly Notices of the Royal Astronomical Society, 350, 914, [arXiv:astro-ph/0303414v2 3.3](#)

- CMB-S4 collaboration, CMB-S4 Science Book, First Edition. 2016, [arXiv:1610.02743](#) 7
- Edmonds, A. R. 1957, Angular Momentum in Quantum Mechanics (Princeton University Press) C
- Essinger-Hileman, T., Kusaka, A., Appel, J. W., et al., Systematic effects from an ambient-temperature, continuously-rotating half-wave plate. 2016, ArXiv e-prints, [arXiv:1601.05901](#) 7
- Fosalba, P., Doré, O., & Bouchet, F. R., Elliptical beams in CMB temperature and polarization anisotropy experiments: An analytic approach. 2002, Phys. Rev. D, 65, 063003, [arXiv:astro-ph/0107346](#) 1, 2, 2
- Górski, K. M., Hivon, E., Banday, A. J., et al., HEALPix: A Framework for High-Resolution Discretization and Fast Analysis of Data Distributed on the Sphere. 2005, ApJ, 622, 759, [arXiv:astro-ph/0409513](#) 2, 2
- Grain, J., Tristram, M., & Stompor, R., Polarized CMB power spectrum estimation using the pure pseudo-cross-spectrum approach. 2009, Phys. Rev. D, 79, 123515, [arXiv:0903.2350](#) 3, 3
- Hansen, F. K. & Górski, K. M., Fast cosmic microwave background power spectrum estimation of temperature and polarization with Gabor transforms. 2003, MNRAS, 343, 559, [arXiv:astro-ph/0207526v1](#) 2, 4
- Hanson, D., Lewis, A., & Challinor, A., Asymmetric Beams and CMB Statistical Anisotropy. 2010, Phys. Rev. D, 81, 103003, [arXiv:1003.0198v2](#) 1
- Hinshaw, G., Nolte, M. R., Bennett, C. L., et al., Three-Year Wilkinson Microwave Anisotropy Probe (WMAP) Observations: Temperature Analysis. 2007, ApJS, 170, 288, [arXiv:astro-ph/0603451v2](#) 1
- Hivon, E., Górski, K. M., Netterfield, C. B., et al., MASTER of the Cosmic Microwave Background Anisotropy Power Spectrum: A Fast Method for Statistical Analysis of Large and Complex Cosmic Microwave Background Data Sets. 2002, ApJ, 567, 2, [arXiv:astro-ph/0105302](#) 2, 4
- Hu, W., Weak lensing of the CMB: A harmonic approach. 2000, Phys. Rev. D, 62, 043007, [arXiv:astro-ph/0001303v1](#) F
- Hu, W., Hedman, M. M., & Zaldarriaga, M., Benchmark parameters for CMB polarization experiments. 2003, Phys. Rev. D, 67, 043004, [arXiv:astro-ph/0210096v1](#) 1, 2, 4
- Johnson, B. R., Collins, J., Abroe, M. E., et al., MAXIPOL: Cosmic Microwave Background Polarimetry Using a Rotating Half-Wave Plate. 2007, Astrophysical Journal, 665, 42, [arXiv:astro-ph/0611394](#) 7
- Keihänen, E. & Reinecke, M., ArtDeco: a beam-deconvolution code for absolute cosmic microwave background measurements. 2012, A&A, 548, 110, [arXiv:1208.1399v2](#) 1
- Leahy, J. P., Bersanelli, M., D'Arcangelo, O., et al., Planck pre-launch status: Expected LFI polarisation capability. 2010, A&A, 520, A8 1
- Lewis, A. & Challinor, A., Weak gravitational lensing of the CMB. 2006, Phys. Rep., 429, 1, [arXiv:astro-ph/0601594v4](#) F
- Miller, N. J., Shimon, M., & Keating, B. G., CMB beam systematics: Impact on lensing parameter estimation. 2009a, Phys. Rev. D, 79, 063008, [arXiv:0806.3096v2](#) 1
- Miller, N. J., Shimon, M., & Keating, B. G., CMB polarization systematics due to beam asymmetry: Impact on cosmological birefringence. 2009b, Phys. Rev. D, 79, 103002, [arXiv:0903.1116v2](#) 1
- Mitra, S., Rocha, G., Górski, K. M., et al., Fast Pixel Space Convolution for Cosmic Microwave Background Surveys with Asymmetric Beams and Complex Scan Strategies: FEBeCoP. 2011, ApJS, 193, 5, [arXiv:1005.1929](#) 1
- Mitra, S., Sengupta, A. S., Ray, S., Saha, R., & Souradeep, T., Cosmic microwave background power spectrum estimation with non-circular beam and incomplete sky coverage. 2009, MNRAS, 394, 1419, [arXiv:astro-ph/0702100v2](#) 1, 3, 3
- Mitra, S., Sengupta, A. S., & Souradeep, T., CMB power spectrum estimation using noncircular beams. 2004, Phys. Rev. D, 70, 103002, [arXiv:astro-ph/0405406v3](#) 1
- O'Dea, D., Challinor, A., & Johnson, B. R., Systematic errors in cosmic microwave background polarization measurements. 2007, MNRAS, 376, 1767, [arXiv:astro-ph/0610361v1](#) 1, 7, 7
- Page, L., Hinshaw, G., Komatsu, E., et al., Three-Year Wilkinson Microwave Anisotropy Probe (WMAP) Observations: Polarization Analysis. 2007, ApJS, 170, 335, [arXiv:astro-ph/0603450v2](#) 1
- Pant, N., Das, S., Rotti, A., Mitra, S., & Souradeep, T., Estimating statistical isotropy violation in CMB due to non-circular beam and complex scan in minutes. 2016, J. Cosmology Astropart. Phys., 3, 035, [arXiv:1511.03672v1](#) 1
- Planck 2013-IV, Planck 2013 results. IV. Low Frequency Instrument beams and window functions. 2014, A&A, 571, A4, [arXiv:1303.5065v2](#) 1, 5
- Planck 2013-VI, Planck 2013 results. VI. High Frequency Instrument data processing. 2014, A&A, 571, A6, [arXiv:1303.5067v3](#) 3
- Planck 2013-VII, Planck 2013 results. VII. HFI time response and beams. 2014, A&A, 571, A7, [arXiv:1303.5068v2](#) 1, 2.1, 2.4, 3.5, 5, F, F
- Planck 2013-VIII, Planck 2013 results. VIII. HFI photometric calibration and mapmaking. 2014, A&A, 571, A8, [arXiv:1303.5069v2](#) 2, 3
- Planck 2013-XVII, Planck 2013 results. XVII. Gravitational lensing by large-scale structure. 2014, A&A, 571, A17, [arXiv:1303.5077v2](#) 1, F
- Planck 2015-VII, Planck 2015 results. VII. HFI data processing: Time-ordered information and beams. 2016, A&A, 594, A7, [arXiv:1502.01586v2](#) 2.1
- Planck 2015-XI, Planck 2015 results. XI. CMB power spectra, likelihoods, and robustness of parameters. 2016, A&A, 594, A11, [arXiv:1507.02704v1](#) 1
- Polarbear Collaboration: Ade, P. A. R., Akiba, Y., Anthony, A. E., et al., A Measurement of the Cosmic Microwave Background B-mode Polarization Power Spectrum at Sub-degree Scales with POLARBEAR. 2014, ApJ, 794, 171, [arXiv:1403.2369](#) 7
- Prézeau, G. & Reinecke, M., Algorithm for the Evaluation of Reduced Wigner Matrices. 2010, ApJS, 190, 267, [arXiv:1002.1050v1](#) 5
- Ramamonjisoa, F. A., Ray, S., Mitra, S., & Souradeep, T., CMB polarization TE power spectrum estimation with non-circular beam. 2013, preprint, [arXiv:1309.4784](#) 1
- Rathaus, B. & Kovetz, E. D., The CMB Derivatives of Planck's Beam Asymmetry. 2014, MNRAS, 443, 750, [arXiv:1405.1609v2](#) 1
- Reinecke, M., Dolag, K., Hell, R., Bartelmann, M., & Enßlin, T. A., A simulation pipeline for the Planck mission. 2006, A&A, 445, 373, [arXiv:astro-ph/0508522v1](#) 5
- Ritacco, A., Adam, R., Adane, A., et al., NIKA 2: next-generation continuum/polarized camera at the IRAM 30 m telescope and its prototype. 2016a, preprint, [arXiv:1602.01605](#) 7
- Ritacco, A., Ponthieu, N., Catalano, A., et al., Polarimetry at millimeter wavelength with NIKA: calibration and performance. 2016b, preprint, [arXiv:1609.02042](#) 7
- Rosset, C., Tristram, M., Ponthieu, N., et al., Planck pre-launch status: High Frequency Instrument polarization calibration. 2010, A&A, 520, A13+, [arXiv:1004.2595](#) 1, 2.1, 2.1, 6
- Rosset, C., Yurchenko, V., Delabrouille, J., et al., Beam mismatch effects in Cosmic Microwave Background polarization measurements. 2007, A&A, 464, 405, [arXiv:astro-ph/0410544v2](#) 1, 5
- Shimon, M., Keating, B., Ponthieu, N., & Hivon, E., CMB polarization systematics due to beam asymmetry: Impact on inflationary science. 2008, Phys. Rev. D, 77, 83003, [arXiv:0709.1513](#) 1, 2.3, 3, 4
- Smith, K. M., Zahn, O., & Doré, O., Detection of gravitational lensing in the cosmic microwave background. 2007, Phys. Rev. D, 76, 043510, [arXiv:0705.3980](#) 1
- Souradeep, T. & Ratra, B., Window Function for Noncircular Beam Cosmic Microwave Background Anisotropy Experiment. 2001, ApJ, 560, 28, [arXiv:astro-ph/0105270v1](#) 1
- Tristram, M., Filliard, C., Perdereau, O., et al., Iterative destripping and photometric calibration for Planck-HFI, polarized, multi-detector map-making. 2011, A&A, 534, A88, [arXiv:1103.2281v2](#) 2, 3, 5
- Tristram, M., Macías-Pérez, J. F., Renault, C., & Hamilton, J.-C., ASYMFASST: A method for convolving maps with asymmetric main beams. 2004, Phys. Rev. D, 69, 123008, [arXiv:astro-ph/0310260v2](#) 2, 2
- Wallis, C. G. R., Bonaldi, A., Brown, M. L., & Battye, R. A., A new map-making algorithm for CMB polarisation experiments. 2015, MNRAS, 453, 2058, [arXiv:1503.03285](#) 1
- Wallis, C. G. R., Brown, M. L., Battye, R. A., Pisano, G., & Lamagna, L., Removing beam asymmetry bias in precision CMB temperature and polarization experiments. 2014, MNRAS, 442, 1963, [arXiv:1401.2075v2](#) 1, 3, 4
- Zaldarriaga, M. & Seljak, U., All-sky analysis of polarization in the microwave background. 1997, Phys. Rev. D, 55, 1830, [arXiv:astro-ph/9609170v2](#) 1, 2, 2, F

Appendix A: Projection of maps on spherical harmonics

Here we give more details on the steps required to go from Eq. (35) to Eq. (38). Let us recall Eq. (35) and explain it further:

$$\tilde{\mathbf{m}}(p) \equiv \begin{pmatrix} \tilde{m}(0; p) \\ \tilde{m}(2; p)/2 \\ \tilde{m}(-2; p)/2 \end{pmatrix}, \quad (\text{A.1})$$

$$\begin{aligned} &= \left(\sum_k \sum_{t \in \mathcal{P}} A_{p,t}^{(k)\dagger} w_k f_{k,t} A_{t,p}^{(k)} \right)^{-1} \left(\sum_j \sum_{t \in \mathcal{P}} A_{p,t}^{(j)\dagger} w_j f_{j,t} d_{j,t} \right), \\ &= \left(\sum_k w_k \begin{pmatrix} \omega_0^{(k)} & \rho_k \omega_{-2}^{(k)} & \rho_k \omega_2^{(k)} \\ \rho_k \omega_2^{(k)} & \rho_k^2 \omega_0^{(k)} & \rho_k^2 \omega_4^{(k)} \\ \rho_k \omega_{-2}^{(k)} & \rho_k^2 \omega_{-4}^{(k)} & \rho_k^2 \omega_0^{(k)} \end{pmatrix} \right)^{-1} \sum_{j \ell m s} w_j (-1)^s q_\ell {}_{-s} Y_{\ell m}(p) \begin{pmatrix} \omega_s^{(j)} \\ \rho_j \omega_{s+2}^{(j)} \\ \rho_j \omega_{s-2}^{(j)} \end{pmatrix} \begin{pmatrix} 0 b_{\ell s}^{(j)*} \\ 2 b_{\ell s}^{(j)*} \\ -2 b_{\ell s}^{(j)*} \end{pmatrix}^T \begin{pmatrix} 0 a_{\ell m} \\ 2 a_{\ell m}/2 \\ -2 a_{\ell m}/2 \end{pmatrix}, \\ &= \sum_{j \ell m s} (-1)^s {}_{-s} Y_{\ell m}(p) \begin{pmatrix} \tilde{\omega}_s^{(j)} \\ \rho_j \tilde{\omega}_{s+2}^{(j)} \\ \rho_j \tilde{\omega}_{s-2}^{(j)} \end{pmatrix} \begin{pmatrix} 0 \hat{b}_{\ell s}^{(j)*} \\ 2 \hat{b}_{\ell s}^{(j)*} \\ -2 \hat{b}_{\ell s}^{(j)*} \end{pmatrix}^T \begin{pmatrix} 0 a_{\ell m} \\ 2 a_{\ell m}/2 \\ -2 a_{\ell m}/2 \end{pmatrix}, \end{aligned} \quad (\text{A.2})$$

where we introduced the s -th complex moment of the direction of polarization for detector j ,

$$\omega_s^{(j)}(p) \equiv \sum_{t \in \mathcal{P}} f_{j,t} e^{i s \alpha_t^{(j)}}, \quad (\text{A.3})$$

the hit matrix \mathbf{H} defined for $(u, v) \in \{0, 2, -2\}^2$ as

$$H_{vu}(p) \equiv \sum_j w_j \omega_{v-u}^{(j)}(p) \rho_{j,v} \rho_{j,u}, \quad (\text{A.4})$$

with

$$\rho_{j,v} \equiv \delta_{v,0} + \rho_j (\delta_{v,-2} + \delta_{v,2}), \quad (\text{A.5})$$

the hit normalized moments

$$\begin{pmatrix} \tilde{\omega}_s^{(j)}(p) \\ \rho_j \tilde{\omega}_{s+2}^{(j)}(p) \\ \rho_j \tilde{\omega}_{s-2}^{(j)}(p) \end{pmatrix} \equiv \mathbf{H}(p)^{-1} \begin{pmatrix} \omega_s^{(j)}(p) \\ \rho_j \omega_{s+2}^{(j)}(p) \\ \rho_j \omega_{s-2}^{(j)}(p) \end{pmatrix} \quad (\text{A.6})$$

which are described in Appendix B, and finally the inverse noise variance weighted beam spherical harmonics (SH) coefficients

$${}_u \hat{b}_{\ell,s}^{(j)} \equiv w_j q_\ell {}_u b_{\ell,s}^{(j)}, \quad (\text{A.7})$$

$$= \rho_j' \hat{b}_{\ell,s+u}^{(j)}. \quad (\text{A.8})$$

Since the solution of Eq. (33) remains the same when all the noise covariances are rescaled simultaneously by an arbitrary factor a : $\mathbf{N}_j \rightarrow a \mathbf{N}_j$, one can also rescale the weights w_j appearing in Eqs (A.4) and (A.7), with for instance $w_j \rightarrow w_j / \sum_k w_k$ without altering the final result.

The components of the observed polarized map are then

$$\tilde{m}(v; p) = \sum_u \frac{k_u}{k_v} \sum_j \sum_s \rho_{j,v} \tilde{\omega}_{s+v}^{(j)}(p) \sum_{\ell m} {}_u a_{\ell m} {}_u \hat{b}_{\ell s}^{(j)*} (-1)^s {}_{-s} Y_{\ell m}(p), \quad (\text{A.9})$$

with

$$k_0 = 1, \quad k_{\pm 2} = 1/2. \quad (\text{A.10})$$

After expansion of the hit normalized moments (Eq. A.6) in spherical harmonics:

$$\tilde{\omega}_{s+v}^{(j)}(p) = \sum_{\ell' m'} {}_{s+v} \tilde{\omega}_{\ell' m'}^{(j)} {}_{s+v} Y_{\ell' m'}(p), \quad (\text{A.11})$$

the polarized map reads

$$\tilde{m}(v; p) = \sum_u \frac{k_u}{k_v} \sum_{j \ell m s \ell' m'} (-1)^s {}_{-s} Y_{\ell m}(p) {}_{s+v} Y_{\ell' m'}(p) {}_u a_{\ell m} {}_u \hat{b}_{\ell s}^{(j)*} \rho_{j,v} {}_{s+v} \tilde{\omega}_{\ell' m'}^{(j)}, \quad (\text{A.12})$$

and the SH coefficients of spin x of map $\tilde{m}(v; p)$ are, for pixels of area Ω_p ,

$${}_x\tilde{m}_{\ell''m''}(v) \equiv \sum_p \Omega_p \tilde{m}(v; p) {}_xY_{\ell''m''}^*(p) = \int d\mathbf{r} \tilde{m}(v; \mathbf{r}) {}_xY_{\ell''m''}^*(\mathbf{r}) \quad (\text{A.13})$$

$$\begin{aligned} &= \sum_u \frac{k_u}{k_v} \sum_j \sum_{\ell m s \ell' m'} (-1)^s {}_u a_{\ell m} {}_u \hat{b}_{\ell s}^{(j)*} \rho_{j,v} {}_{s+v} \tilde{\omega}_{\ell' m'}^{(j)} \int d\mathbf{r} {}_{-s} Y_{\ell m}(\mathbf{r}) {}_{s+v} Y_{\ell' m'}(\mathbf{r}) {}_x Y_{\ell'' m''}^*(\mathbf{r}) \\ &= \sum_u \frac{k_u}{k_v} \sum_{j \ell m s \ell' m'} {}_u a_{\ell m} {}_u \hat{b}_{\ell s}^{(j)*} \rho_{j,v} {}_{s+v} \tilde{\omega}_{\ell' m'}^{(j)} (-1)^{s+x+m'+\ell+\ell'+\ell''} \left[\frac{(2\ell+1)(2\ell'+1)(2\ell''+1)}{4\pi} \right]^{1/2} \begin{pmatrix} \ell & \ell' & \ell'' \\ m & m' & -m'' \end{pmatrix} \begin{pmatrix} \ell & \ell' & \ell'' \\ -s & s+v & -x \end{pmatrix} \end{aligned} \quad (\text{A.14})$$

which are only non-zero when $x = v$. The cross power spectrum of spin v_1 and v_2 maps is then given by Eq. (38).

Appendix B: Hit matrix

Introducing, for detector j ,

$$\mathbf{H}_s^{(j)} = \begin{pmatrix} \omega_s^{(j)} & \rho_j \omega_{s-2}^{(j)} & \rho_j \omega_{s+2}^{(j)} \\ \rho_j \omega_{s+2}^{(j)} & \rho_j^2 \omega_s^{(j)} & \rho_j^2 \omega_{s+4}^{(j)} \\ \rho_j \omega_{s-2}^{(j)} & \rho_j^2 \omega_{s-4}^{(j)} & \rho_j^2 \omega_s^{(j)} \end{pmatrix}, \quad (\text{B.1})$$

the Hermitian hit matrix for a weighted combination of detectors is

$$\mathbf{H} \equiv \sum_j w_j \mathbf{H}_0^{(j)}, \quad (\text{B.2})$$

$$= h \begin{pmatrix} 1 & \bar{z}_2 & z_2 \\ z_2 & x & z_4 \\ \bar{z}_2 & \bar{z}_4 & x \end{pmatrix}, \quad (\text{B.3})$$

with h, x real and z_2, z_4 complex numbers, and has for inverse

$$\mathbf{H}^{-1} = \frac{1}{h\Delta} \begin{pmatrix} x^2 - |z_4|^2 & z_2 \bar{z}_4 - x \bar{z}_2 & \bar{z}_2 z_4 - x z_2 \\ \bar{z}_2 z_4 - x z_2 & x - |z_2|^2 & z_2^2 - z_4 \\ z_2 \bar{z}_4 - x \bar{z}_2 & z_2^2 - \bar{z}_4 & x - |z_2|^2 \end{pmatrix}, \quad (\text{B.4})$$

with

$$\Delta = x^2 - 2x|z_2|^2 - |z_4|^2 + z_2^2 \bar{z}_4 + \bar{z}_2^2 z_4. \quad (\text{B.5})$$

In Eq. (A.6) we defined

$$\begin{pmatrix} \tilde{\omega}_s^{(j)}[0] \\ \rho_j \tilde{\omega}_{s+2}^{(j)}[2] \\ \rho_j \tilde{\omega}_{s-2}^{(j)}[-2] \end{pmatrix} \equiv \mathbf{H}^{-1} \begin{pmatrix} \omega_s^{(j)} \\ \rho_j \omega_{s+2}^{(j)} \\ \rho_j \omega_{s-2}^{(j)} \end{pmatrix} \quad (\text{B.6})$$

for any value of s , which provides

$$\begin{pmatrix} \tilde{\omega}_s^{(j)}[0] \\ \rho_j \tilde{\omega}_s^{(j)}[2] \\ \rho_j \tilde{\omega}_s^{(j)}[-2] \end{pmatrix} = \frac{1}{h\Delta} \begin{pmatrix} (x^2 - |z_4|^2) \omega_s^{(j)} + (z_2 \bar{z}_4 - x \bar{z}_2) \rho_j \omega_{s+2}^{(j)} + (\bar{z}_2 z_4 - x z_2) \rho_j \omega_{s-2}^{(j)} \\ (x - |z_2|^2) \rho_j \omega_s^{(j)} + (\bar{z}_2 z_4 - x z_2) \omega_{s-2}^{(j)} + (z_2^2 - z_4) \rho_j \omega_{s-4}^{(j)} \\ (x - |z_2|^2) \rho_j \omega_s^{(j)} + (z_2 \bar{z}_4 - x \bar{z}_2) \omega_{s+2}^{(j)} + (\bar{z}_2^2 - \bar{z}_4) \rho_j \omega_{s+4}^{(j)} \end{pmatrix}, \quad (\text{B.7})$$

so that $\tilde{\omega}_s^{(j)}$ is of spin s , provided z_2 and z_4 are of spin 2 and 4 respectively. Since $\omega_s^{(j)} = \omega_{-s}^{(j)*}$, we get $\tilde{\omega}_s^{(j)*}[2] = \tilde{\omega}_{-s}^{(j)}[-2]$.

By definition,

$$\begin{pmatrix} \tilde{\omega}_s^{(j)}[0] & \rho_j \tilde{\omega}_{s-2}^{(j)}[0] & \rho_j \tilde{\omega}_{s+2}^{(j)}[0] \\ \rho_j \tilde{\omega}_{s+2}^{(j)}[2] & \rho_j^2 \tilde{\omega}_s^{(j)}[2] & \rho_j^2 \tilde{\omega}_{s+4}^{(j)}[2] \\ \rho_j \tilde{\omega}_{s-2}^{(j)}[-2] & \rho_j^2 \tilde{\omega}_{s-4}^{(j)}[-2] & \rho_j^2 \tilde{\omega}_s^{(j)}[-2] \end{pmatrix} = \mathbf{H}^{-1} \cdot \mathbf{H}_s^{(j)} \quad (\text{B.8})$$

so that

$$\sum_j w_j \begin{pmatrix} \tilde{\omega}_0^{(j)}[0] & \rho_j \tilde{\omega}_{-2}^{(j)}[0] & \rho_j \tilde{\omega}_2^{(j)}[0] \\ \rho_j \tilde{\omega}_2^{(j)}[2] & \rho_j^2 \tilde{\omega}_0^{(j)}[2] & \rho_j^2 \tilde{\omega}_4^{(j)}[2] \\ \rho_j \tilde{\omega}_{-2}^{(j)}[-2] & \rho_j^2 \tilde{\omega}_{-4}^{(j)}[-2] & \rho_j^2 \tilde{\omega}_0^{(j)}[-2] \end{pmatrix} = \begin{pmatrix} 1 & 0 & 0 \\ 0 & 1 & 0 \\ 0 & 0 & 1 \end{pmatrix}. \quad (\text{B.9})$$

Appendix C: Wigner 3J symbols

The Wigner 3J symbols describe the coupling between different spin weighted spherical harmonics at the same location:

$${}_s Y_{\ell_1 m_1}(\mathbf{r}) {}_s Y_{\ell_2 m_2}(\mathbf{r}) = \sum_{\ell_3 s_3 m_3} \left(\frac{(2\ell_1 + 1)(2\ell_2 + 1)(2\ell_3 + 1)}{4\pi} \right)^{1/2} \begin{pmatrix} \ell_1 & \ell_2 & \ell_3 \\ m_1 & m_2 & m_3 \end{pmatrix} \begin{pmatrix} \ell_1 & \ell_2 & \ell_3 \\ -s_1 & -s_2 & -s_3 \end{pmatrix} {}_s Y_{\ell_3 m_3}^*(\mathbf{r}) \quad (\text{C.1})$$

and the symbol $\begin{pmatrix} \ell_1 & \ell_2 & \ell_3 \\ m_1 & m_2 & m_3 \end{pmatrix}$ is non-zero only when, $|m_i| \leq \ell_i$ for $i = 1, 2, 3$, $m_1 + m_2 + m_3 = 0$ and

$$|\ell_1 - \ell_2| \leq \ell_3 \leq \ell_1 + \ell_2. \quad (\text{C.2})$$

They obey the relations

$$\begin{pmatrix} \ell_1 & \ell_2 & \ell_3 \\ -m_1 & -m_2 & -m_3 \end{pmatrix} = (-1)^{\ell_1 + \ell_2 + \ell_3} \begin{pmatrix} \ell_1 & \ell_2 & \ell_3 \\ m_1 & m_2 & m_3 \end{pmatrix}, \quad (\text{C.3})$$

and

$$\begin{pmatrix} \ell & \ell & 0 \\ m & -m & 0 \end{pmatrix} = \frac{(-1)^{\ell-m}}{\sqrt{2\ell+1}}. \quad (\text{C.4})$$

Their standard orthogonality relations are

$$\sum_{\ell_3} (2\ell_3 + 1) \begin{pmatrix} \ell_1 & \ell_2 & \ell_3 \\ m_1 & m_2 & m_3 \end{pmatrix} \begin{pmatrix} \ell_1 & \ell_2 & \ell_3 \\ m'_1 & m'_2 & m'_3 \end{pmatrix} = \delta_{m_1 m'_1} \delta_{m_2 m'_2}, \quad (\text{C.5})$$

and

$$\sum_{m_1 m_2} \begin{pmatrix} \ell_1 & \ell_2 & \ell_3 \\ m_1 & m_2 & m_3 \end{pmatrix} \begin{pmatrix} \ell_1 & \ell_2 & \ell'_3 \\ m_1 & m_2 & m'_3 \end{pmatrix} = \delta_{\ell_3 \ell'_3} \delta_{m_3 m'_3} \frac{\delta(\ell_1, \ell_2, \ell_3)}{2\ell_3 + 1}, \quad (\text{C.6})$$

where $\delta(\ell_1, \ell_2, \ell_3) = 1$ when ℓ_1, ℓ_2, ℓ_3 obey the triangle relation of Eq. (C.2) and vanishes otherwise.

For $\ell_1 \ll \ell_2, \ell_3$ (Edmonds 1957, Eq. A2.1)

$$\begin{pmatrix} \ell_1 & \ell_2 & \ell_3 \\ m_1 & m_2 & -m_1 - m_2 \end{pmatrix} \simeq \frac{(-1)^{\ell_3 + m_2 + m_1}}{\sqrt{2\ell_3 + 1}} d_{\ell_3 - \ell_2, m_1}^{\ell_1}(\theta), \quad (\text{C.7})$$

where d is the Wigner rotation matrix and $\cos \theta = 2m_2 / (2\ell_2 + 1)$. As a consequence, for $|m_2| \ll \ell_2$

$$\begin{pmatrix} \ell_1 & \ell_2 & \ell_3 \\ m_1 & m_2 & -m_1 - m_2 \end{pmatrix} \simeq (-1)^{m_2 - m'_2} \begin{pmatrix} \ell_1 & \ell_2 & \ell_3 \\ m_1 & m'_2 & -m_1 - m'_2 \end{pmatrix}, \quad (\text{C.8})$$

and an approximate orthogonality relation can therefore be written, for $\ell_1, |m_1|, |m_2| \ll \ell_2, \ell_3$

$$\sum_{\ell_3} (2\ell_3 + 1) \begin{pmatrix} \ell_1 & \ell_2 & \ell_3 \\ m_1 & m_2 & m_3 \end{pmatrix} \begin{pmatrix} \ell_1 & \ell_2 & \ell_3 \\ m'_1 & m'_2 & m'_3 \end{pmatrix} \simeq (-1)^{m_2 - m'_2} \delta_{m_1 m'_1}. \quad (\text{C.9})$$

Appendix D: Spin weighted power spectra

Since a complex field of spin s can be written as $C_s = R_s + iI_s$ where R_s and I_s are real, with

$$R_s \pm iI_s = \sum_{\ell m} {}_{\pm s} a_{\ell m} {}_{\pm s} Y_{\ell m} \quad (\text{D.1})$$

and, with the Condon-Shortley phase convention ${}_s Y_{\ell m}^* = (-1)^{s+m} {}_{-s} Y_{\ell -m}$, then

$${}_s a_{\ell m}^* = (-1)^{s+m} {}_{-s} a_{\ell -m}. \quad (\text{D.2})$$

When $s = 2$, one defines

$$a_{\ell m}^E = -({}_2 a_{\ell m} + {}_{-2} a_{\ell m}) / 2 \quad (\text{D.3a})$$

$$a_{\ell m}^B = -({}_2 a_{\ell m} - {}_{-2} a_{\ell m}) / (2i) \quad (\text{D.3b})$$

such that $a_{\ell m}^{X*} = (-1)^m a_{\ell -m}^X$, with $X = E, B$, and

$$C_{\ell}^{EE} = (C_{\ell}^{22} + C_{\ell}^{2-2} + C_{\ell}^{-22} + C_{\ell}^{-2-2}) / 4, \quad (\text{D.4a})$$

$$C_{\ell}^{BB} = (C_{\ell}^{22} - C_{\ell}^{2-2} - C_{\ell}^{-22} + C_{\ell}^{-2-2}) / 4, \quad (\text{D.4b})$$

$$C_{\ell}^{EB} = -(C_{\ell}^{22} - C_{\ell}^{2-2} + C_{\ell}^{-22} - C_{\ell}^{-2-2}) / (4i). \quad (\text{D.4c})$$

When $s = 1$, one defines

$$a_{\ell m}^G = -({}_1 a_{\ell m} - {}_{-1} a_{\ell m})/2 \quad (\text{D.5a})$$

$$a_{\ell m}^C = -({}_1 a_{\ell m} + {}_{-1} a_{\ell m})/(2i) \quad (\text{D.5b})$$

such that $a_{\ell m}^{X*} = (-1)^m a_{\ell -m}^X$, with $X = G, C$, and

$$C_\ell^{GG} = (C_\ell^{11} - C_\ell^{1-1} - C_\ell^{-11} + C_\ell^{-1-1})/4, \quad (\text{D.6a})$$

$$C_\ell^{CC} = (C_\ell^{11} + C_\ell^{1-1} + C_\ell^{-11} + C_\ell^{-1-1})/4, \quad (\text{D.6b})$$

$$C_\ell^{GC} = -(C_\ell^{11} + C_\ell^{1-1} - C_\ell^{-11} - C_\ell^{-1-1})/(4i). \quad (\text{D.6c})$$

Appendix E: Window matrices $W_\ell^{XY, X'Y'}$

E.1. Arbitrary beams, smooth scanning case

Let us come back to Eqs. (39) and (40). These can be cast in a more compact matrix form

$$\bar{\mathbf{C}}_\ell = \sum_{j_1 j_2} \sum_s \{ [\mathbf{D}^{-1} \cdot \hat{\mathbf{B}}_{\ell, s}^{(j_1)\dagger} \cdot \mathbf{D} \cdot \mathbf{C}_\ell \cdot \mathbf{D} \cdot \hat{\mathbf{B}}_{\ell, s}^{(j_2)} \cdot \mathbf{D}^{-1}] * \bar{\mathbf{\Omega}}_s^{(j_1 j_2)} \} \quad (\text{E.1})$$

where

$$\mathbf{C}_\ell \equiv \begin{pmatrix} C_\ell^{00} & C_\ell^{02} & C_\ell^{0-2} \\ C_\ell^{20} & C_\ell^{22} & C_\ell^{2-2} \\ C_\ell^{-20} & C_\ell^{-22} & C_\ell^{-2-2} \end{pmatrix}, \quad (\text{E.2})$$

$$\mathbf{D} \equiv \begin{pmatrix} 1 & 0 & 0 \\ 0 & 1/2 & 0 \\ 0 & 0 & 1/2 \end{pmatrix}, \quad (\text{E.3})$$

$$\hat{\mathbf{B}}_{\ell, s}^{(j)} \equiv \begin{pmatrix} 0 \hat{b}_{\ell, s}^{(j)} & 0 \hat{b}_{\ell, s-2}^{(j)} & 0 \hat{b}_{\ell, s+2}^{(j)} \\ 2 \hat{b}_{\ell, s}^{(j)} & 2 \hat{b}_{\ell, s-2}^{(j)} & 2 \hat{b}_{\ell, s+2}^{(j)} \\ -2 \hat{b}_{\ell, s}^{(j)} & -2 \hat{b}_{\ell, s-2}^{(j)} & -2 \hat{b}_{\ell, s+2}^{(j)} \end{pmatrix} = \begin{pmatrix} \hat{b}_{\ell, s}^{(j)} & \hat{b}_{\ell, s-2}^{(j)} & \hat{b}_{\ell, s+2}^{(j)} \\ \rho'_j \hat{b}_{\ell, s+2}^{(j)} & \rho'_j \hat{b}_{\ell, s}^{(j)} & \rho'_j \hat{b}_{\ell, s+4}^{(j)} \\ \rho'_j \hat{b}_{\ell, s-2}^{(j)} & \rho'_j \hat{b}_{\ell, s-4}^{(j)} & \rho'_j \hat{b}_{\ell, s}^{(j)} \end{pmatrix}, \quad (\text{E.4})$$

and $\mathbf{X} * \mathbf{Y}$ denotes the elementwise product (also known as Hadamard or Schur product) of arrays \mathbf{X} and \mathbf{Y} . Noting that

$$\begin{pmatrix} C_\ell^{00} & C_\ell^{02} & C_\ell^{0-2} \\ C_\ell^{20} & C_\ell^{22} & C_\ell^{2-2} \\ C_\ell^{-20} & C_\ell^{-22} & C_\ell^{-2-2} \end{pmatrix} = \mathbf{R}_2 \cdot \begin{pmatrix} C_\ell^{TT} & C_\ell^{TE} & C_\ell^{TB} \\ C_\ell^{ET} & C_\ell^{EE} & C_\ell^{EB} \\ C_\ell^{BT} & C_\ell^{BE} & C_\ell^{BB} \end{pmatrix} \cdot \mathbf{R}_2^\dagger \quad (\text{E.5})$$

where \mathbf{R}_2 was introduced in Eq. (18), which leads to Eq. (41) that we recall here for convenience:

$$\bar{\mathbf{C}}_\ell^{XY} = \sum_{X'Y'} W_\ell^{XY, X'Y'} C_\ell^{X'Y'}. \quad (\text{E.6})$$

Introducing the short-hand

$$\hat{\mathbf{\Omega}}_{v_1 v_2}^s \equiv \bar{\mathbf{\Omega}}_{v_1, v_2, s}^{(j_1 j_2)}, \quad (\text{E.7})$$

describing the coupled moments of the polarized detectors j_1 and j_2 orientation, and assuming in Eq. (E.4) the beams to be perfectly co-polarized, with polar efficiencies ρ'_j , one gets, for $XY = TT, EE, BB, TE, TB, EB, ET, BT, BE$:

$$W_\ell^{XY, TT} = \sum_s \sum_{j_1 j_2} \begin{pmatrix} \hat{\mathbf{\Omega}}_{00}^s \hat{b}_{\ell, s}^{(j_1)*} \hat{b}_{\ell, s}^{(j_2)} \\ \hat{b}_{\ell, s+2}^{(j_1)*} \left(\hat{\mathbf{\Omega}}_{-2-2}^s \hat{b}_{\ell, s+2}^{(j_2)} + \hat{\mathbf{\Omega}}_{-22}^s \hat{b}_{\ell, s-2}^{(j_2)} \right) + \hat{b}_{\ell, s-2}^{(j_1)*} \left(\hat{\mathbf{\Omega}}_{2-2}^s \hat{b}_{\ell, s+2}^{(j_2)} + \hat{\mathbf{\Omega}}_{22}^s \hat{b}_{\ell, s-2}^{(j_2)} \right) \\ \hat{b}_{\ell, s+2}^{(j_1)*} \left(\hat{\mathbf{\Omega}}_{-2-2}^s \hat{b}_{\ell, s+2}^{(j_2)} - \hat{\mathbf{\Omega}}_{-22}^s \hat{b}_{\ell, s-2}^{(j_2)} \right) + \hat{b}_{\ell, s-2}^{(j_1)*} \left(\hat{\mathbf{\Omega}}_{22}^s \hat{b}_{\ell, s-2}^{(j_2)} - \hat{\mathbf{\Omega}}_{2-2}^s \hat{b}_{\ell, s+2}^{(j_2)} \right) \\ - \hat{b}_{\ell, s}^{(j_1)*} \left(\hat{\mathbf{\Omega}}_{0-2}^s \hat{b}_{\ell, s+2}^{(j_2)} + \hat{\mathbf{\Omega}}_{02}^s \hat{b}_{\ell, s-2}^{(j_2)} \right) \\ - i \hat{b}_{\ell, s}^{(j_1)*} \left(\hat{\mathbf{\Omega}}_{02}^s \hat{b}_{\ell, s-2}^{(j_2)} - \hat{\mathbf{\Omega}}_{0-2}^s \hat{b}_{\ell, s+2}^{(j_2)} \right) \\ i \hat{b}_{\ell, s+2}^{(j_1)*} \left(\hat{\mathbf{\Omega}}_{-22}^s \hat{b}_{\ell, s-2}^{(j_2)} - \hat{\mathbf{\Omega}}_{-2-2}^s \hat{b}_{\ell, s+2}^{(j_2)} \right) + i \hat{b}_{\ell, s-2}^{(j_1)*} \left(\hat{\mathbf{\Omega}}_{22}^s \hat{b}_{\ell, s-2}^{(j_2)} - \hat{\mathbf{\Omega}}_{2-2}^s \hat{b}_{\ell, s+2}^{(j_2)} \right) \\ - \hat{b}_{\ell, s}^{(j_2)} \left(\hat{\mathbf{\Omega}}_{-20}^s \hat{b}_{\ell, s+2}^{(j_1)*} + \hat{\mathbf{\Omega}}_{20}^s \hat{b}_{\ell, s-2}^{(j_1)*} \right) \\ - i \hat{b}_{\ell, s}^{(j_2)} \left(\hat{\mathbf{\Omega}}_{-20}^s \hat{b}_{\ell, s+2}^{(j_1)*} - \hat{\mathbf{\Omega}}_{20}^s \hat{b}_{\ell, s-2}^{(j_1)*} \right) \\ i \hat{b}_{\ell, s+2}^{(j_1)*} \left(\hat{\mathbf{\Omega}}_{-2-2}^s \hat{b}_{\ell, s+2}^{(j_2)} + \hat{\mathbf{\Omega}}_{-22}^s \hat{b}_{\ell, s-2}^{(j_2)} \right) - i \hat{b}_{\ell, s-2}^{(j_1)*} \left(\hat{\mathbf{\Omega}}_{2-2}^s \hat{b}_{\ell, s+2}^{(j_2)} + \hat{\mathbf{\Omega}}_{22}^s \hat{b}_{\ell, s-2}^{(j_2)} \right) \end{pmatrix}, \quad (\text{E.8a})$$

which is illustrated in Fig. 3;

$$W_{\ell}^{XY, EE} = \sum_s \sum_{j_1 j_2} \frac{\rho'_{j_1} \rho'_{j_2}}{4} \left(\begin{array}{l} \hat{\Omega}_{\ell, s-2}^s (\hat{b}_{\ell, s-2}^{(j_1)*} + \hat{b}_{\ell, s+2}^{(j_1)*}) (\hat{b}_{\ell, s-2}^{(j_2)} + \hat{b}_{\ell, s+2}^{(j_2)}) \\ \hat{b}_{\ell, s}^{(j_1)*} \left[\hat{b}_{\ell, s}^{(j_2)} (\hat{\Omega}_{-2-2}^s + \hat{\Omega}_{-22}^s + \hat{\Omega}_{2-2}^s + \hat{\Omega}_{22}^s) + \hat{b}_{\ell, s+4}^{(j_2)} (\hat{\Omega}_{-2-2}^s + \hat{\Omega}_{2-2}^s) + \hat{b}_{\ell, s-4}^{(j_2)} (\hat{\Omega}_{-22}^s + \hat{\Omega}_{22}^s) \right] \\ + \hat{b}_{\ell, s+4}^{(j_1)*} \left[\hat{b}_{\ell, s}^{(j_2)} (\hat{\Omega}_{-2-2}^s + \hat{\Omega}_{2-2}^s) + \hat{\Omega}_{-2-2}^s \hat{b}_{\ell, s+4}^{(j_2)} + \hat{\Omega}_{2-2}^s \hat{b}_{\ell, s-4}^{(j_2)} \right] \\ + \hat{b}_{\ell, s-4}^{(j_1)*} \left[\hat{b}_{\ell, s}^{(j_2)} (\hat{\Omega}_{-2-2}^s + \hat{\Omega}_{2-2}^s) + \hat{\Omega}_{-2-2}^s \hat{b}_{\ell, s+4}^{(j_2)} + \hat{\Omega}_{2-2}^s \hat{b}_{\ell, s-4}^{(j_2)} \right] \\ \hat{b}_{\ell, s}^{(j_1)*} \left[\hat{b}_{\ell, s}^{(j_2)} (\hat{\Omega}_{-2-2}^s - \hat{\Omega}_{2-2}^s - \hat{\Omega}_{-22}^s + \hat{\Omega}_{22}^s) + \hat{b}_{\ell, s+4}^{(j_2)} (\hat{\Omega}_{-2-2}^s - \hat{\Omega}_{2-2}^s) + \hat{b}_{\ell, s-4}^{(j_2)} (\hat{\Omega}_{22}^s - \hat{\Omega}_{-22}^s) \right] \\ + \hat{b}_{\ell, s+4}^{(j_1)*} \left[\hat{b}_{\ell, s}^{(j_2)} (\hat{\Omega}_{-2-2}^s - \hat{\Omega}_{2-2}^s) + \hat{\Omega}_{-2-2}^s \hat{b}_{\ell, s+4}^{(j_2)} - \hat{\Omega}_{2-2}^s \hat{b}_{\ell, s-4}^{(j_2)} \right] \\ + \hat{b}_{\ell, s-4}^{(j_1)*} \left[\hat{b}_{\ell, s}^{(j_2)} (\hat{\Omega}_{22}^s - \hat{\Omega}_{-22}^s) - \hat{\Omega}_{2-2}^s \hat{b}_{\ell, s+4}^{(j_2)} + \hat{\Omega}_{22}^s \hat{b}_{\ell, s-4}^{(j_2)} \right] \\ - (\hat{b}_{\ell, s-2}^{(j_1)*} + \hat{b}_{\ell, s+2}^{(j_1)*}) \left[\hat{b}_{\ell, s}^{(j_2)} (\hat{\Omega}_{0-2}^s + \hat{\Omega}_{02}^s) + \hat{\Omega}_{0-2}^s \hat{b}_{\ell, s+4}^{(j_2)} + \hat{\Omega}_{02}^s \hat{b}_{\ell, s-4}^{(j_2)} \right] \\ - i (\hat{b}_{\ell, s-2}^{(j_1)*} + \hat{b}_{\ell, s+2}^{(j_1)*}) \left[\hat{b}_{\ell, s}^{(j_2)} (\hat{\Omega}_{02}^s - \hat{\Omega}_{0-2}^s) - \hat{\Omega}_{0-2}^s \hat{b}_{\ell, s+4}^{(j_2)} + \hat{\Omega}_{02}^s \hat{b}_{\ell, s-4}^{(j_2)} \right] \\ i \hat{b}_{\ell, s}^{(j_1)*} \left[\hat{b}_{\ell, s}^{(j_2)} (-\hat{\Omega}_{-2-2}^s + \hat{\Omega}_{-22}^s - \hat{\Omega}_{2-2}^s + \hat{\Omega}_{22}^s) - \hat{b}_{\ell, s+4}^{(j_2)} (\hat{\Omega}_{-2-2}^s + \hat{\Omega}_{2-2}^s) + \hat{b}_{\ell, s-4}^{(j_2)} (\hat{\Omega}_{-22}^s + \hat{\Omega}_{22}^s) \right] \\ + i \hat{b}_{\ell, s+4}^{(j_1)*} \left[\hat{b}_{\ell, s}^{(j_2)} (\hat{\Omega}_{-22}^s - \hat{\Omega}_{-2-2}^s) - \hat{\Omega}_{-2-2}^s \hat{b}_{\ell, s+4}^{(j_2)} + \hat{\Omega}_{2-2}^s \hat{b}_{\ell, s-4}^{(j_2)} \right] \\ + i \hat{b}_{\ell, s-4}^{(j_1)*} \left[\hat{b}_{\ell, s}^{(j_2)} (\hat{\Omega}_{22}^s - \hat{\Omega}_{2-2}^s) - \hat{\Omega}_{2-2}^s \hat{b}_{\ell, s+4}^{(j_2)} + \hat{\Omega}_{22}^s \hat{b}_{\ell, s-4}^{(j_2)} \right] \\ - (\hat{b}_{\ell, s-2}^{(j_2)} + \hat{b}_{\ell, s+2}^{(j_2)}) \left[(\hat{\Omega}_{-20}^s + \hat{\Omega}_{20}^s) \hat{b}_{\ell, s}^{(j_1)*} + \hat{\Omega}_{-20}^s \hat{b}_{\ell, s+4}^{(j_1)*} + \hat{\Omega}_{20}^s \hat{b}_{\ell, s-4}^{(j_1)*} \right] \\ i (\hat{b}_{\ell, s-2}^{(j_2)} + \hat{b}_{\ell, s+2}^{(j_2)}) \left[(\hat{\Omega}_{20}^s - \hat{\Omega}_{-20}^s) \hat{b}_{\ell, s}^{(j_1)*} - \hat{\Omega}_{20}^s \hat{b}_{\ell, s+4}^{(j_1)*} + \hat{\Omega}_{-20}^s \hat{b}_{\ell, s-4}^{(j_1)*} \right] \\ i \hat{b}_{\ell, s}^{(j_1)*} \left[\hat{b}_{\ell, s}^{(j_2)} (\hat{\Omega}_{-2-2}^s + \hat{\Omega}_{-22}^s - \hat{\Omega}_{2-2}^s - \hat{\Omega}_{22}^s) + \hat{b}_{\ell, s+4}^{(j_2)} (\hat{\Omega}_{-2-2}^s - \hat{\Omega}_{2-2}^s) + \hat{b}_{\ell, s-4}^{(j_2)} (\hat{\Omega}_{-22}^s - \hat{\Omega}_{22}^s) \right] \\ + i \hat{b}_{\ell, s+4}^{(j_1)*} \left[\hat{b}_{\ell, s}^{(j_2)} (\hat{\Omega}_{-2-2}^s + \hat{\Omega}_{-22}^s) + \hat{\Omega}_{-2-2}^s \hat{b}_{\ell, s+4}^{(j_2)} + \hat{\Omega}_{2-2}^s \hat{b}_{\ell, s-4}^{(j_2)} \right] \\ - i \hat{b}_{\ell, s-4}^{(j_1)*} \left[\hat{b}_{\ell, s}^{(j_2)} (\hat{\Omega}_{2-2}^s + \hat{\Omega}_{22}^s) + \hat{\Omega}_{2-2}^s \hat{b}_{\ell, s+4}^{(j_2)} + \hat{\Omega}_{22}^s \hat{b}_{\ell, s-4}^{(j_2)} \right] \end{array} \right), \quad (\text{E.8b})$$

$$W_{\ell}^{XY, TE} = \sum_s \sum_{j_1 j_2} \frac{\rho'_{j_2}}{2} \left(\begin{array}{l} -\hat{\Omega}_{00}^s \hat{b}_{\ell, s}^{(j_1)*} (\hat{b}_{\ell, s-2}^{(j_2)} + \hat{b}_{\ell, s+2}^{(j_2)}) \\ -\hat{b}_{\ell, s+2}^{(j_1)*} \left[\hat{b}_{\ell, s}^{(j_2)} (\hat{\Omega}_{-2-2}^s + \hat{\Omega}_{-22}^s) + \hat{\Omega}_{-2-2}^s \hat{b}_{\ell, s+4}^{(j_2)} + \hat{\Omega}_{-22}^s \hat{b}_{\ell, s-4}^{(j_2)} \right] \\ -\hat{b}_{\ell, s-2}^{(j_1)*} \left[\hat{b}_{\ell, s}^{(j_2)} (\hat{\Omega}_{-2-2}^s + \hat{\Omega}_{22}^s) + \hat{\Omega}_{-2-2}^s \hat{b}_{\ell, s+4}^{(j_2)} + \hat{\Omega}_{22}^s \hat{b}_{\ell, s-4}^{(j_2)} \right] \\ -\hat{b}_{\ell, s+2}^{(j_1)*} \left[\hat{b}_{\ell, s}^{(j_2)} (\hat{\Omega}_{-2-2}^s - \hat{\Omega}_{-22}^s) + \hat{\Omega}_{-2-2}^s \hat{b}_{\ell, s+4}^{(j_2)} - \hat{\Omega}_{-22}^s \hat{b}_{\ell, s-4}^{(j_2)} \right] \\ -\hat{b}_{\ell, s-2}^{(j_1)*} \left[\hat{b}_{\ell, s}^{(j_2)} (\hat{\Omega}_{22}^s - \hat{\Omega}_{2-2}^s) - \hat{\Omega}_{2-2}^s \hat{b}_{\ell, s+4}^{(j_2)} + \hat{\Omega}_{22}^s \hat{b}_{\ell, s-4}^{(j_2)} \right] \\ \hat{b}_{\ell, s}^{(j_1)*} \left[\hat{b}_{\ell, s}^{(j_2)} (\hat{\Omega}_{0-2}^s + \hat{\Omega}_{02}^s) + \hat{\Omega}_{0-2}^s \hat{b}_{\ell, s+4}^{(j_2)} + \hat{\Omega}_{02}^s \hat{b}_{\ell, s-4}^{(j_2)} \right] \\ i \hat{b}_{\ell, s}^{(j_1)*} \left[\hat{b}_{\ell, s}^{(j_2)} (\hat{\Omega}_{02}^s - \hat{\Omega}_{0-2}^s) - \hat{\Omega}_{0-2}^s \hat{b}_{\ell, s+4}^{(j_2)} + \hat{\Omega}_{02}^s \hat{b}_{\ell, s-4}^{(j_2)} \right] \\ -i \hat{b}_{\ell, s+2}^{(j_1)*} \left[\hat{b}_{\ell, s}^{(j_2)} (\hat{\Omega}_{-22}^s - \hat{\Omega}_{-2-2}^s) - \hat{\Omega}_{-2-2}^s \hat{b}_{\ell, s+4}^{(j_2)} + \hat{\Omega}_{-22}^s \hat{b}_{\ell, s-4}^{(j_2)} \right] \\ -i \hat{b}_{\ell, s-2}^{(j_1)*} \left[\hat{b}_{\ell, s}^{(j_2)} (\hat{\Omega}_{22}^s - \hat{\Omega}_{2-2}^s) - \hat{\Omega}_{2-2}^s \hat{b}_{\ell, s+4}^{(j_2)} + \hat{\Omega}_{22}^s \hat{b}_{\ell, s-4}^{(j_2)} \right] \\ (\hat{b}_{\ell, s-2}^{(j_2)} + \hat{b}_{\ell, s+2}^{(j_2)}) (\hat{\Omega}_{-20}^s \hat{b}_{\ell, s+2}^{(j_1)*} + \hat{\Omega}_{20}^s \hat{b}_{\ell, s-2}^{(j_1)*}) \\ -i (\hat{b}_{\ell, s-2}^{(j_2)} + \hat{b}_{\ell, s+2}^{(j_2)}) (\hat{\Omega}_{20}^s \hat{b}_{\ell, s-2}^{(j_1)*} - \hat{\Omega}_{-20}^s \hat{b}_{\ell, s+2}^{(j_1)*}) \\ -i \hat{b}_{\ell, s+2}^{(j_1)*} \left[\hat{b}_{\ell, s}^{(j_2)} (\hat{\Omega}_{-2-2}^s + \hat{\Omega}_{-22}^s) + \hat{\Omega}_{-2-2}^s \hat{b}_{\ell, s+4}^{(j_2)} + \hat{\Omega}_{-22}^s \hat{b}_{\ell, s-4}^{(j_2)} \right] \\ + i \hat{b}_{\ell, s-2}^{(j_1)*} \left[\hat{b}_{\ell, s}^{(j_2)} (\hat{\Omega}_{2-2}^s + \hat{\Omega}_{22}^s) + \hat{\Omega}_{2-2}^s \hat{b}_{\ell, s+4}^{(j_2)} + \hat{\Omega}_{22}^s \hat{b}_{\ell, s-4}^{(j_2)} \right] \end{array} \right). \quad (\text{E.8c})$$

Since, by definition (Eqs. A.7 and E.7), $\hat{b}_{\ell, s}^{(j)*} = (-1)^s \hat{b}_{\ell, -s}^{(j)}$ and $\hat{\Omega}_{v_1 v_2}^{s*} = \hat{\Omega}_{-v_1, -v_2}^{-s}$, one can check that each term of $W_{\ell}^{XY, X'Y'}$ is real, as expected.

E.2. Arbitrary beams, ideal scanning

In the case of ideal scanning described in Section 3.4, one gets $\omega_s^{(j)}(p) = \delta_{s,0} h(p)$, so that the hit matrix is diagonal:

$$\mathbf{H}(p) = h(p) \sum_j \begin{pmatrix} w_j & 0 & 0 \\ 0 & w_j \rho_j^2 & 0 \\ 0 & 0 & w_j \rho_j^2 \end{pmatrix}, \quad (\text{E.9})$$

and the orientation moments

$$\tilde{\omega}_s^{(j)}[0] = \delta_{s,0} \left(\sum_k w_k \right)^{-1}, \quad \tilde{\omega}_s^{(j)}[\pm 2] = \delta_{s,0} \left(\sum_k w_k \rho_k^2 \right)^{-1}, \quad (\text{E.10})$$

are such that

$$\hat{\Omega}_{v_1 v_2}^s = \begin{pmatrix} \xi_{00} & \rho_{j_2} \xi_{02} & \rho_{j_2} \xi_{02} \\ \rho_{j_1} \xi_{20} & \rho_{j_1} \rho_{j_2} \xi_{22} & \rho_{j_1} \rho_{j_2} \xi_{22} \\ \rho_{j_1} \xi_{20} & \rho_{j_1} \rho_{j_2} \xi_{22} & \rho_{j_1} \rho_{j_2} \xi_{22} \end{pmatrix} \delta_{s,0}, \quad (\text{E.11})$$

with

$$\xi_{00}^{-1} = \sum_{k_1 k_2} w_{k_1} w_{k_2}, \quad \xi_{02}^{-1} = \sum_{k_1 k_2} w_{k_1} w_{k_2} \rho_{k_2}^2, \quad \xi_{20}^{-1} = \sum_{k_1 k_2} w_{k_1} w_{k_2} \rho_{k_1}^2, \quad \xi_{22}^{-1} = \sum_{k_1 k_2} w_{k_1} w_{k_2} \rho_{k_1}^2 \rho_{k_2}^2. \quad (\text{E.12})$$

One then obtains the beam matrices

$$W_\ell^{XY, TT} = \sum_{j_1 j_2} \begin{pmatrix} \hat{b}_{\ell,0}^{(j_2)} \hat{b}_{\ell,0}^{(j_1)*} \xi_{00} \\ (\hat{b}_{\ell,-2}^{(j_2)} + \hat{b}_{\ell,2}^{(j_2)}) (\hat{b}_{\ell,-2}^{(j_1)*} + \hat{b}_{\ell,2}^{(j_1)*}) \rho_{j_1} \rho_{j_2} \xi_{22} \\ (\hat{b}_{\ell,-2}^{(j_2)} - \hat{b}_{\ell,2}^{(j_2)}) (\hat{b}_{\ell,-2}^{(j_1)*} - \hat{b}_{\ell,2}^{(j_1)*}) \rho_{j_1} \rho_{j_2} \xi_{22} \\ -(\hat{b}_{\ell,-2}^{(j_2)} + \hat{b}_{\ell,2}^{(j_2)}) \hat{b}_{\ell,0}^{(j_1)*} \rho_{j_2} \xi_{02} \\ -i(\hat{b}_{\ell,-2}^{(j_2)} - \hat{b}_{\ell,2}^{(j_2)}) \hat{b}_{\ell,0}^{(j_1)*} \rho_{j_2} \xi_{02} \\ i(\hat{b}_{\ell,-2}^{(j_2)} - \hat{b}_{\ell,2}^{(j_2)}) (\hat{b}_{\ell,-2}^{(j_1)*} + \hat{b}_{\ell,2}^{(j_1)*}) \rho_{j_1} \rho_{j_2} \xi_{22} \\ -\hat{b}_{\ell,0}^{(j_2)} (\hat{b}_{\ell,-2}^{(j_1)*} + \hat{b}_{\ell,2}^{(j_1)*}) \rho_{j_1} \xi_{20} \\ i\hat{b}_{\ell,0}^{(j_2)} (\hat{b}_{\ell,-2}^{(j_1)*} - \hat{b}_{\ell,2}^{(j_1)*}) \rho_{j_1} \xi_{20} \\ -i(\hat{b}_{\ell,-2}^{(j_2)} + \hat{b}_{\ell,2}^{(j_2)}) (\hat{b}_{\ell,-2}^{(j_1)*} - \hat{b}_{\ell,2}^{(j_1)*}) \rho_{j_1} \rho_{j_2} \xi_{22} \end{pmatrix}, \quad (\text{E.13a})$$

$$W_\ell^{XY, EE} = \sum_{j_1 j_2} \frac{\rho_{j_1}' \rho_{j_2}'}{4} \begin{pmatrix} (\hat{b}_{\ell,-2}^{(j_2)} + \hat{b}_{\ell,2}^{(j_2)}) (\hat{b}_{\ell,-2}^{(j_1)*} + \hat{b}_{\ell,2}^{(j_1)*}) \xi_{00} \\ (\hat{b}_{\ell,-4}^{(j_2)} + 2\hat{b}_{\ell,0}^{(j_2)} + \hat{b}_{\ell,4}^{(j_2)}) (\hat{b}_{\ell,-4}^{(j_1)*} + 2\hat{b}_{\ell,0}^{(j_1)*} + \hat{b}_{\ell,4}^{(j_1)*}) \rho_{j_1} \rho_{j_2} \xi_{22} \\ (\hat{b}_{\ell,-4}^{(j_2)} - \hat{b}_{\ell,4}^{(j_2)}) (\hat{b}_{\ell,-4}^{(j_1)*} - \hat{b}_{\ell,4}^{(j_1)*}) \rho_{j_1} \rho_{j_2} \xi_{22} \\ -(\hat{b}_{\ell,-4}^{(j_2)} + 2\hat{b}_{\ell,0}^{(j_2)} + \hat{b}_{\ell,4}^{(j_2)}) (\hat{b}_{\ell,-2}^{(j_1)*} + \hat{b}_{\ell,2}^{(j_1)*}) \rho_{j_2} \xi_{02} \\ -i(\hat{b}_{\ell,-4}^{(j_2)} - \hat{b}_{\ell,4}^{(j_2)}) (\hat{b}_{\ell,-2}^{(j_1)*} + \hat{b}_{\ell,2}^{(j_1)*}) \rho_{j_2} \xi_{02} \\ i(\hat{b}_{\ell,-4}^{(j_2)} - \hat{b}_{\ell,4}^{(j_2)}) (\hat{b}_{\ell,-4}^{(j_1)*} + 2\hat{b}_{\ell,0}^{(j_1)*} + \hat{b}_{\ell,4}^{(j_1)*}) \rho_{j_1} \rho_{j_2} \xi_{22} \\ -(\hat{b}_{\ell,-2}^{(j_2)} + \hat{b}_{\ell,2}^{(j_2)}) (\hat{b}_{\ell,-4}^{(j_1)*} + 2\hat{b}_{\ell,0}^{(j_1)*} + \hat{b}_{\ell,4}^{(j_1)*}) \rho_{j_1} \xi_{20} \\ i(\hat{b}_{\ell,-2}^{(j_2)} + \hat{b}_{\ell,2}^{(j_2)}) (\hat{b}_{\ell,-4}^{(j_1)*} - \hat{b}_{\ell,4}^{(j_1)*}) \rho_{j_1} \xi_{20} \\ -i(\hat{b}_{\ell,-4}^{(j_2)} + 2\hat{b}_{\ell,0}^{(j_2)} + \hat{b}_{\ell,4}^{(j_2)}) (\hat{b}_{\ell,-4}^{(j_1)*} - \hat{b}_{\ell,4}^{(j_1)*}) \rho_{j_1} \rho_{j_2} \xi_{22} \end{pmatrix}, \quad (\text{E.13b})$$

$$W_\ell^{XY, TE} = \sum_{j_1 j_2} \frac{\rho_{j_2}'}{2} \begin{pmatrix} -(\hat{b}_{\ell,-2}^{(j_2)} + \hat{b}_{\ell,2}^{(j_2)}) \hat{b}_{\ell,0}^{(j_1)*} \xi_{00} \\ -(\hat{b}_{\ell,-4}^{(j_2)} + 2\hat{b}_{\ell,0}^{(j_2)} + \hat{b}_{\ell,4}^{(j_2)}) (\hat{b}_{\ell,-2}^{(j_1)*} + \hat{b}_{\ell,2}^{(j_1)*}) \rho_{j_1} \rho_{j_2} \xi_{22} \\ -(\hat{b}_{\ell,-4}^{(j_2)} - \hat{b}_{\ell,4}^{(j_2)}) (\hat{b}_{\ell,-2}^{(j_1)*} - \hat{b}_{\ell,2}^{(j_1)*}) \rho_{j_1} \rho_{j_2} \xi_{22} \\ (\hat{b}_{\ell,-4}^{(j_2)} + 2\hat{b}_{\ell,0}^{(j_2)} + \hat{b}_{\ell,4}^{(j_2)}) \hat{b}_{\ell,0}^{(j_1)*} \rho_{j_2} \xi_{02} \\ i(\hat{b}_{\ell,-4}^{(j_2)} - \hat{b}_{\ell,4}^{(j_2)}) \hat{b}_{\ell,0}^{(j_1)*} \rho_{j_2} \xi_{02} \\ -i(\hat{b}_{\ell,-4}^{(j_2)} - \hat{b}_{\ell,4}^{(j_2)}) (\hat{b}_{\ell,-2}^{(j_1)*} + \hat{b}_{\ell,2}^{(j_1)*}) \rho_{j_1} \rho_{j_2} \xi_{22} \\ (\hat{b}_{\ell,-2}^{(j_2)} + \hat{b}_{\ell,2}^{(j_2)}) (\hat{b}_{\ell,-2}^{(j_1)*} + \hat{b}_{\ell,2}^{(j_1)*}) \rho_{j_1} \xi_{20} \\ -i(\hat{b}_{\ell,-2}^{(j_2)} + \hat{b}_{\ell,2}^{(j_2)}) (\hat{b}_{\ell,-2}^{(j_1)*} - \hat{b}_{\ell,2}^{(j_1)*}) \rho_{j_1} \xi_{20} \\ i(\hat{b}_{\ell,-4}^{(j_2)} + 2\hat{b}_{\ell,0}^{(j_2)} + \hat{b}_{\ell,4}^{(j_2)}) (\hat{b}_{\ell,-2}^{(j_1)*} - \hat{b}_{\ell,2}^{(j_1)*}) \rho_{j_1} \rho_{j_2} \xi_{22} \end{pmatrix}. \quad (\text{E.13c})$$

The implications of Eq. (E.13) are discussed in Section 3.4.

Appendix F: Finite pixel size

Introducing the spin raising and lowering differential operators applied to a function f of spin s , (Zaldarriaga & Seljak 1997; Bunn et al. 2003, and references therein)

$$\delta f = -\sin^s \theta \left(\frac{\partial}{\partial \theta} + \frac{i}{\sin \theta} \frac{\partial}{\partial \varphi} \right) [\sin^{-s} \theta f] = s \cot \theta f - \frac{\partial f}{\partial \theta} - \frac{i}{\sin \theta} \frac{\partial f}{\partial \varphi} \quad (\text{F.1})$$

$$\bar{\delta} f = -\sin^{-s} \theta \left(\frac{\partial}{\partial \theta} - \frac{i}{\sin \theta} \frac{\partial}{\partial \varphi} \right) [\sin^s \theta f] = -s \cot \theta f - \frac{\partial f}{\partial \theta} + \frac{i}{\sin \theta} \frac{\partial f}{\partial \varphi} \quad (\text{F.2})$$

the spin weighed spherical harmonics are defined as

$${}_s Y_{\ell m} \equiv \sqrt{\frac{(\ell - s)!}{(\ell + s)!}} \delta^s Y_{\ell m}, \quad 0 \leq s \leq \ell; \quad (\text{F.3})$$

$${}_s Y_{\ell m} \equiv (-1)^s \sqrt{\frac{(\ell + s)!}{(\ell - s)!}} \bar{\delta}^{-s} Y_{\ell m}, \quad -\ell \leq s \leq 0; \quad (\text{F.4})$$

such that

$$\delta_s Y_{\ell m} = f(\ell, s) {}_{s+1}Y_{\ell m}, \quad (\text{F.5})$$

$$\bar{\delta}_s Y_{\ell m} = -f(\ell, -s) {}_{s-1}Y_{\ell m}, \quad (\text{F.6})$$

with $f(\ell, s) = \sqrt{(\ell-s)(\ell+s+1)} = \sqrt{\ell(\ell+1) - s(s+1)}$.

As noticed in [Planck 2013-VII \(2014\)](#) and [Planck 2013-XVII \(2014\)](#), the formalism of subpixel effect is very close to the one of gravitational lensing described in [Hu \(2000\)](#) and [Lewis & Challinor \(2006\)](#).

For $\mathbf{r} = (1, \theta, \varphi) = \mathbf{e}_r$ and $d\mathbf{r} = (0, d\theta, d\varphi) = d\theta \mathbf{e}_\theta + \sin\theta d\varphi \mathbf{e}_\varphi$,

$${}_s Y_{\ell m}(\mathbf{r} + d\mathbf{r}) = {}_s Y_{\ell m}(\mathbf{r}) + d\mathbf{r} \cdot \nabla {}_s Y_{\ell m}(\mathbf{r}) + \frac{1}{2} \sum_{ij} d\mathbf{r}_i d\mathbf{r}_j \nabla_i \nabla_j {}_s Y_{\ell m}(\mathbf{r}) \quad (\text{F.7})$$

$$= {}_s Y_{\ell m}(\mathbf{r}) - \frac{1}{2} (\bar{d}\mathbf{r} \delta + d\mathbf{r} \bar{\delta}) {}_s Y_{\ell m}(\mathbf{r}) + \frac{1}{8} (\bar{d}\mathbf{r} \bar{d}\mathbf{r} \delta \delta + \bar{d}\mathbf{r} d\mathbf{r} \delta \bar{\delta} + d\mathbf{r} \bar{d}\mathbf{r} \delta \delta + d\mathbf{r} d\mathbf{r} \bar{\delta} \bar{\delta}) {}_s Y_{\ell m}(\mathbf{r}) \quad (\text{F.8})$$

$$= {}_s Y_{\ell m}(\mathbf{r}) - \frac{1}{2} (\bar{d}\mathbf{r} f(\ell, s) {}_{s+1}Y_{\ell m}(\mathbf{r}) - d\mathbf{r} f(\ell, -s) {}_{s-1}Y_{\ell m}(\mathbf{r})) - \frac{1}{4} d\mathbf{r} \bar{d}\mathbf{r} (\ell(\ell+1) - s^2) {}_s Y_{\ell m}(\mathbf{r}) \\ + \frac{1}{8} (\bar{d}\mathbf{r} \bar{d}\mathbf{r} g(\ell, s) {}_{s+2}Y_{\ell m}(\mathbf{r}) + d\mathbf{r} d\mathbf{r} g(\ell, -s) {}_{s-2}Y_{\ell m}(\mathbf{r})) \quad (\text{F.9})$$

with $d\mathbf{r} = d\mathbf{r} \cdot (\mathbf{e}_\theta + i\mathbf{e}_\varphi) = d\theta + i \sin\theta d\varphi$, $\bar{d}\mathbf{r} = d\theta - i \sin\theta d\varphi$ and $g(\ell, s) = f(\ell, s)f(\ell, s+1)$.

Identifying $d\mathbf{r}$ to the position of a measurement relative to the nominal center \mathbf{r} of the pixel to which it is attributed, this expansion of ${}_s Y_{\ell m}$ can be injected into Eqs. (28) and (A.14). Assuming $d\mathbf{r}$ to be uncorrelated with the orientation of the detector, two extra terms, both quadratic in $d\mathbf{r}$, will appear in the final power spectra.

The first term involves the scalar product of the gradient of the signal in the pixel, assumed to be totally dominated by the temperature, with the weighted sum of $d\mathbf{r}$ over all samples in that pixel. Introducing

$$\rho_{j,v} \bar{\omega}_{s+v}^{(j)\pm}(p) = \sum_{v'} (\mathbf{H}^{-1}(p))_{vv'} \rho_{j,v'} \sum_{t \in p} (d\theta_t \pm i \sin\theta_t d\varphi_t) f_{j,t} e^{i(s+v')\alpha_t^{(j)}} \quad (\text{F.10})$$

which is of spin $s+v \pm 1$ and such that $(\rho_{j,v} \bar{\omega}_{s+v}^{(j)+})^* = \rho_{j,-v} \bar{\omega}_{-s-v}^{(j)-}$, one finds

$$\Delta \bar{C}_{\ell'}^{v_1 v_2} = \frac{1}{k_{v_1} k_{v_2}} \sum_{s_1 s_2} (-1)^{s_1+s_2} \sum_{j_1 j_2 \ell} \ell(\ell+1) \frac{2\ell+1}{4\pi} C_\ell^{TT} \hat{b}_{\ell s_1}^{(j_1)*} \hat{b}_{\ell s_2}^{(j_2)} \\ \times \sum_{\ell'} \frac{2\ell'+1}{4} \left[D_{s_1+v_1, s_2+v_2, \ell'}^{(j_1 j_2)++} J_{s_1+1, s_2+1}^{v_1, v_2} + D_{s_1+v_1, s_2+v_2, \ell'}^{(j_1 j_2)--} J_{s_1-1, s_2-1}^{v_1, v_2} - D_{s_1+v_1, s_2+v_2, \ell'}^{(j_1 j_2)+-} J_{s_1+1, s_2-1}^{v_1, v_2} - D_{s_1+v_1, s_2+v_2, \ell'}^{(j_1 j_2)-+} J_{s_1-1, s_2+1}^{v_1, v_2} \right] \quad (\text{F.11})$$

with

$$D_{s_1+v_1, s_2+v_2, \ell'}^{(j_1 j_2)\sigma_1 \sigma_2} = \rho_{j_1, v_1} \rho_{j_2, v_2} \frac{1}{2\ell'+1} \sum_{m'} {}_{s_1+v_1} \bar{\omega}_{\ell' m'}^{(j_1)\sigma_1} {}_{s_2+v_2} \bar{\omega}_{\ell' m'}^{(j_2)\sigma_2*} \quad \text{with } \{\sigma_1, \sigma_2\} \in \{+, -\}, \quad (\text{F.12})$$

$$J_{s_1+\sigma_1, s_2+\sigma_2}^{v_1, v_2} = \begin{pmatrix} \ell & \ell' & \ell'' \\ -s_1 - \sigma_1 & s_1 + \sigma_1 + v_1 & -v_1 \end{pmatrix} \begin{pmatrix} \ell & \ell' & \ell'' \\ -s_2 - \sigma_2 & s_2 + \sigma_2 + v_2 & -v_2 \end{pmatrix} \quad \text{with } \{\sigma_1, \sigma_2\} \in \{+1, -1\}. \quad (\text{F.13})$$

In the case of temperature, and assuming the beams to be circular, this simplifies to

$$\Delta \bar{C}_{\ell'}^{TT} = \sum_{j_1 j_2 \ell} \ell(\ell+1) \frac{2\ell+1}{4\pi} C_\ell^{TT} \hat{b}_{\ell 0}^{(j_1)*} \hat{b}_{\ell 0}^{(j_2)} \\ \times \sum_{\ell'} \frac{2\ell'+1}{4} \begin{pmatrix} \ell & \ell' & \ell'' \\ 1 & -1 & 0 \end{pmatrix}^2 \left[(D_{00, \ell'}^{(j_1 j_2)++} + D_{00, \ell'}^{(j_1 j_2)--}) - (-1)^{\ell+\ell'+\ell''} (D_{00, \ell'}^{(j_1 j_2)+-} + D_{00, \ell'}^{(j_1 j_2)-+}) \right] \quad (\text{F.14})$$

in agreement with [Planck 2013-VII \(2014\)](#), once one identifies $(D_{00, \ell'}^{(j_1 j_2)++} + D_{00, \ell'}^{(j_1 j_2)--})/2$ as the sum of the gradient and curl parts of the (spin 1) displacement field power spectrum and $-(D_{00, \ell'}^{(j_1 j_2)+-} + D_{00, \ell'}^{(j_1 j_2)-+})/2$ as their difference (see Section D).

It is instructive to further assume the relative location of the hit's center of mass to be only weakly correlated between pixels, so that all its derived power spectra can be assumed to be white: $D_{s_1+v_1, s_2+v_2, \ell'}^{(j_1 j_2)\sigma_1 \sigma_2} = D_{s_1+v_1, s_2+v_2}^{(j_1 j_2)\sigma_1 \sigma_2}$ (i.e., with a variance $D_{s_1+v_1, s_2+v_2}^{(j_1 j_2)\sigma_1 \sigma_2} / \Omega_{\text{pix}}$ in pixels of solid angle $\Omega_{\text{pix}} = 4\pi/N_{\text{pix}}$). Equation (C.5) then ensures that the sub-pixel noise of Eq. (F.11) is also white, with constant polarized spectra

$$\Delta \bar{C}_{\ell'}^{XY} = N^{XY} = \sum_{\ell} \ell(\ell+1) \frac{2\ell+1}{4\pi} C_\ell^{TT} \mathcal{W}_\ell^{XY} \quad (\text{F.15})$$

with

$$\mathcal{W}_\ell^{TT} = \frac{1}{4} \sum_{j_1 j_2 s} (\hat{b}_{\ell s}^{(j_1)*} \hat{b}_{\ell s}^{(j_2)} [D_{ss}^{(j_1 j_2)++} + D_{ss}^{(j_1 j_2)--}] + \hat{b}_{\ell s}^{(j_1)*} \hat{b}_{\ell, s+2}^{(j_2)} D_{s, s+2}^{(j_1 j_2)+-} + \hat{b}_{\ell, s+2}^{(j_1)*} \hat{b}_{\ell s}^{(j_2)} D_{s+2, s}^{(j_1 j_2)-+}), \quad (\text{F.16})$$

$$\simeq \frac{1}{4} \sum_{j_1 j_2} \hat{b}_{\ell 0}^{(j_1)*} \hat{b}_{\ell 0}^{(j_2)} [D_{00}^{(j_1 j_2)++} + D_{00}^{(j_1 j_2)--}]; \quad (\text{F.17})$$

$$\mathcal{W}_\ell^{EE} = \mathcal{W}_\ell^{BB} = \frac{1}{4} \sum_{j_1 j_2 s} \sum_{v=-2,2} (\hat{b}_{\ell s}^{(j_1)*} \hat{b}_{\ell s}^{(j_2)} [D_{s+v, s+v}^{(j_1 j_2)++} + D_{s+v, s+v}^{(j_1 j_2)--}] + \hat{b}_{\ell s}^{(j_1)*} \hat{b}_{\ell, s+2}^{(j_2)} D_{s+v, s+2+v}^{(j_1 j_2)+-} + \hat{b}_{\ell, s+2}^{(j_1)*} \hat{b}_{\ell s}^{(j_2)} D_{s+2+v, s+v}^{(j_1 j_2)-+}), \quad (\text{F.18})$$

$$\simeq \frac{1}{4} \sum_{j_1 j_2} \hat{b}_{\ell 0}^{(j_1)*} \hat{b}_{\ell 0}^{(j_2)} [D_{22}^{(j_1 j_2)++} + D_{22}^{(j_1 j_2)--} + D_{-2-2}^{(j_1 j_2)++} + D_{-2-2}^{(j_1 j_2)--}]; \quad (\text{F.19})$$

$$\mathcal{W}_\ell^{XY} = 0 \quad \text{when } X \neq Y \quad (\text{F.20})$$

where the approximate results are obtained for circular beams.

Even for more realistic hypotheses on the hits locations, the sub-pixel contributions to the respective power spectra follow the hierarchy

$$\Delta \tilde{C}_\ell^{TT} \sim \Delta \tilde{C}_\ell^{EE} \sim \Delta \tilde{C}_\ell^{BB} \gg \Delta \tilde{C}_\ell^{TE} \sim \Delta \tilde{C}_\ell^{TB} \sim \Delta \tilde{C}_\ell^{EB}. \quad (\text{F.21})$$

Let us consider now the other extra contribution to the power spectrum, involving the Laplacian of the sky signal and the quadratic norm of \mathbf{dr} . Introducing

$$\rho_{j,v} \tilde{\omega}_v^{(j)'}(p) = \sum_{v'} (\mathbf{H}^{-1}(p))_{vv'} \rho_{j,v'} \sum_{t \in p} (d\theta_t^2 + \sin^2 \theta_t d\varphi_t^2) f_{j,t} e^{iv' \alpha_t^{(j)}} \quad (\text{F.22})$$

$$\simeq \sigma_p^2 \rho_{j,v} \tilde{\omega}_v^{(j)}(p) \quad (\text{F.23})$$

where σ_p^2 is the second order moment of the hit location in pixel p . If we assume this and $\tilde{\omega}_v^{(j)}(p)$ to be slowly varying functions of p , and consider $\ell \gg s$, the power spectra become

$$C_\ell \longrightarrow \left(1 - \frac{1}{2} \ell(\ell+1) \sigma^2\right) C_\ell \quad (\text{F.24})$$

which describes to leading order, the smoothing effect of the integration of the signal on the pixel.

Appendix G: Co-polarized beam

For an arbitrarily shaped beam having the intensity harmonics coefficients

$$b_{\ell m} = \int \mathbf{dr} \tilde{I}(\mathbf{r}) Y_{\ell m}^*(\mathbf{r}), \quad (\text{G.1})$$

and assumed to be perfectly co-polarized in direction γ , its polarized harmonics' content will be

$$\pm_2 b_{\ell m} = \int \mathbf{dr} (\tilde{Q}(\mathbf{r}) \pm i \tilde{U}(\mathbf{r})) \pm_2 Y_{\ell m}^*(\mathbf{r}) = \int \mathbf{dr} \tilde{I}(\mathbf{r}) e^{\pm 2i(\gamma - \varphi_r)} \pm_2 Y_{\ell m}^*(\mathbf{r}) \quad (\text{G.2})$$

$$= e^{\pm 2i\gamma} \sum_{\ell' m'} b_{\ell' m'} \int_0^{2\pi} d\varphi \int_0^\pi d\theta \sin \theta e^{\mp 2i\varphi_r} Y_{\ell' m'}(\theta, \varphi) \pm_2 Y_{\ell m}^*(\theta, \varphi) \quad (\text{G.3})$$

$$= e^{\pm 2i\gamma} 2\pi \sum_{\ell'} b_{\ell', m \pm 2} (-1)^m \sum_{\ell'' \geq 2} \left(\frac{(2\ell+1)(2\ell'+1)(2\ell''+1)}{4\pi} \right)^{1/2} \begin{pmatrix} \ell & \ell' & \ell'' \\ -m & m \pm 2 & \mp 2 \end{pmatrix} \begin{pmatrix} \ell & \ell' & \ell'' \\ \pm 2 & 0 & \mp 2 \end{pmatrix} I_{\ell''} \quad (\text{G.4})$$

where we used Eq. (C.1) and introduced, for $\ell'' \geq 2$

$$I_{\ell''} \equiv \int_0^\pi d\theta \sin \theta \pm_2 Y_{\ell'', \mp 2}^*(\theta), \quad (\text{G.5})$$

$$= \sqrt{\frac{2\ell''+1}{4\pi}} \int_0^\pi d\theta \sin \theta d_{\mp 2, \mp 2}^{\ell''}(\theta), \quad (\text{G.6})$$

$$= \sqrt{\frac{2\ell''+1}{4\pi}} \frac{4}{\ell''(\ell''+1)} (-1)^{\ell''}. \quad (\text{G.7})$$

Since $I_{\ell''}$ peaks at $\ell'' = 2$, the 3J symbols will enforce $\ell'' \ll \ell \simeq \ell'$ in Eq. (G.4). If the beam is narrow enough in real space, $b_{\ell',m}$ will be almost constant over the allowed range $\ell - \ell'' \leq \ell' \leq \ell + \ell''$, and we use the approximate orthogonality relation of Eq. (C.9) to write

$$\begin{aligned} \sum_{\ell'} b_{\ell',m\pm 2} (-1)^m \sqrt{(2\ell+1)(2\ell'+1)} \begin{pmatrix} \ell & \ell' & \ell'' \\ -m & m\pm 2 & \mp 2 \end{pmatrix} \begin{pmatrix} \ell & \ell' & \ell'' \\ \pm 2 & 0 & \mp 2 \end{pmatrix} &\simeq b_{\ell,m\pm 2} \sum_{\ell'} (-1)^m (2\ell'+1) (-1)^{m\pm 2} \begin{pmatrix} \ell & \ell' & \ell'' \\ \pm 2 & 0 & \mp 2 \end{pmatrix}^2, \\ &= b_{\ell,m\pm 2}. \end{aligned} \quad (\text{G.8})$$

Finally, we note that in Eq. (G.4), the sum

$$2\pi \sum_{\ell''=2}^{2n+1} \sqrt{\frac{2\ell''+1}{4\pi}} I_{\ell''} = \sum_{\ell''=2}^{2n+1} (-1)^{\ell''} \frac{2(2\ell''+1)}{\ell''(\ell''+1)}, \quad (\text{G.9})$$

$$= \sum_{p=1}^n \frac{1}{p(p+1)} = \sum_{p=1}^n \frac{1}{p} - \frac{1}{p+1}, \quad (\text{G.10})$$

$$= 1 - \frac{1}{n+1}, \quad (\text{G.11})$$

to obtain

$${}_{\pm 2} b_{\ell m} = e^{\pm 2i\gamma} b_{\ell, m\pm 2}, \quad (\text{G.12})$$

which is valid for any (narrow) co-polarized beam.